APPLICATION OF SIMUFACT IN SIMULATING THE ACTUAL MAXIMUM STRESS IN A TUNGSTEN INERT GAS WELDMENT

BY

OLUYOH EDIRIN

ENG2002692

DEPARTMENT OF PRODUCTION ENGINEERING,

FACULTY OF ENGINEERING

UNIVERSITY OF BENIN,BENIN CITY.

SEPTEMPBER, 2025

APPLICATION OF SIMUFACT IN SIMULATING THE ACTUAL MAXIMUM STRESS IN A TUNGSTEN INERT GAS WELDMENT

BY

OLUYOH EDIRIN

ENG2002692

A RESEARCH PROJECT WRITTEN AND SUBMITTED TO THE DEPARTMENT OF PRODUCTION ENGINEERING, FACULTY OF ENGINEERING, UNIVERSITY OF BENIN, IN PARTIAL FULFILMENT OF THE REQUIREMENTS FOR DEGREE OF BACHELOR OF ENGINEERING OF THE UNIVERSITY OF BENIN, BENIN CITY

DECLARATION

I declare that:

This project work is based on a study undertaken by me in the Department of Production Engineering, University of Benin under the supervision of Engr. Dr.B.O ERHUNMWUNSE. This work has not been previously submitted for award of a degree elsewhere.

All ideas and views are products of my personal research effort and all references to works of others have been duly acknowledged .

_____

OLUYOH EDIRIN

DATE:_____

CERTIFICATION

We certify that OLUYOH EDIRIN with the matriculation number ENG2002692 submitted the research work to the department of production engineering, Faculty of Engineering, University of Benin City.

_____ _____

Engr. Dr. B.O ERHUNMWUNSE DATE

Project supervisor

_____ _____

Engr Dr E.M. ETUK DATE

Project coordinator

_____ _____ Prof

P.E. AMIOLEMHEN DATE

Head of department

DEDICATION

This project is wholeheartedly dedicated to my beloved parents, whose unwavering love, constant encourageent, and sacrifices have been the foundation of all my achievements. Their prayers, guidance, and support have been my strength throughout this academic journey. Without them, this work would not have been possible.

ACKNOWLEDGEMENTS

First and foremost, I give all glory to God Almighty for the strength, wisdom, and perseverance granted to me throughout the course of this project.

I would like to express my deepest gratitude to my project supervisor, Engr. Dr. B.O. Erhunmwunse, for his exceptional guidance, valuable suggestions, and unwavering support. His mentorship, patience, and insightful feedback were instrumental to the successful completion of this research work.

I am especially thankful to my parents, Engr. Godwin Oluyoh and Mrs. Ejiro Oluyoh, whose love, prayers, and encouragement have been the foundation of my academic journey. Their constant motivation and sacrifices have shaped who I am today, and for that, I am eternally grateful.

To everyone who contributed in one way or another to the success of this project, I sincerely appreciate you.

TABLE OF CONTENTS

LIST OF TABLES

LIST OF FIGURES

ABSTRACT

This study investigates the simulation of the actual maximum stress in Tungsten Inert Gas (TIG) weldment using SIMUFACT Welding software. The research aimed to compare the simulated stress values with experimental results obtained in a controlled environment under varying process parameters such as current, voltage, and gas flow rate.

During the design of experiment, twenty experimental runs was generated by the Central composite design and it was used to carry out TIG welding on mild steel plates. A universal testing machine was used to record the actual maximumm stress on the welded joint and recorded as experimental values. The data generated from the CCD matrix was then feed into an expert system (SIMUFACT 2024) which was used to carry out TIG welding simulations with its corresponding actual maximum stress recorded alongside as the SIMUFACT result.

Results from this study revealed that that increasing welding current reduces the maximum stress due to higher heat input and lower cooling rate, while voltage variation influences arc width and stress distribution. The actual maximum stress values from both datasets were analyzed and compared. The results revealed close agreement between experimental and simulated values, a fitted line plot was used to ascertain the degree of correlation between both results and a correlation coefficient of 0.98 was observed, indicating a very strong positive correlation degree between the experimental result and the SIMUFACT result. A time series plot was then used to compare if both data sets assumed the same trend. The SIMUFACT welding simulation analysis proved to be a reliable tool for simulating and predicting the actual maximum stress in TIG-welded joints thereby aiding in the optimization of welding parameters for an improved structural integrity.

CHAPTER ONE

INTRODUCTION

1.1 BACKGROUND TO THE STUDY

Welding is a fundamental manufacturing process used for joining metals and thermoplastics through fusion or solid-state bonding. It plays a crucial role in high-integrity industries such as aerospace, automotive, and pressure vessel fabrication, where the reliability of joints is vital for ensuring structural performance (Kou, 2003; Pandey *et al*., 2021). Despite its numerous advantages, welding introduces thermo-metallurgical changes that can degrade the mechanical properties of the weld zone, often making it the primary site of failure under operational stresses (Messler, 2008; Kumar, 2020).

Welding methods are broadly classified into fusion welding and solid-state welding. Solid-state welding techniques, such as friction stir welding and ultrasonic welding, achieve bonding without melting the base materials, relying instead on mechanisms like plastic deformation and atomic diffusion to form the joint (Kalpakjian and Schmid, 2014; Messler, 2008). In contrast, fusion welding involves melting the base metals to create a joint through the solidification of the molten pool. Common examples of fusion welding include Gas Metal Arc Welding (GMAW), Shielded Metal Arc Welding (SMAW), Submerged Arc Welding (SAW), and Tungsten Inert Gas (TIG) welding. Each of these techniques differs in terms of heat input, weld quality, metallurgical influence, and material compatibility.

TIG welding (also known as Gas Tungsten Arc Welding, GTAW) employs a non-consumable tungsten electrode and an inert shielding gas (typically argon or helium) to produce high-purity welds with precise heat control. This makes TIG welding particularly suitable for welding thin sections and reactive alloys, such as aluminum and titanium, although it requires a high level of skill and is generally slower than other welding methods (Kou, 2003; Sathiya *et al*., 2019).

The localized heating and cooling cycles in TIG welding generate significant residual stresses due to the constrained thermal expansion and contraction of the material. These stresses can lead to distortion, cracking, and accelerated fatigue failure, which ultimately compromise the structural integrity of the welded joint (Lindgren, 2001; Deng, 2018).

To address these challenges, various advanced simulation techniques have been developed. For instance, Computational Fluid Dynamics (CFD) is used to model the weld pool dynamics, including fluid flow, heat transfer, and mass transport in the molten weld pool. Microstructure Evolution Modeling predicts phase transformations in the weld zone, while Machine Learning (ML)-augmented simulations offer new approaches for optimizing welding parameters. Among the most effective tools for simulating the thermomechanical processes of welding is SIMUFACT software. This computational tool provides high-fidelity simulations of welding processes by modeling temperature-dependent material behavior and transient thermal cycles. It predicts residual stress distributions, identifies critical stress zones, and helps optimize welding parameters to improve the overall quality of the weld (Goldak and Akhlaghi, 2005; Muránsky *et al*., 2019).

1.2 STATEMENT OF THE PROBLEM

Residual stresses induced during welding processes remain a major challenge in structural integrity assessment. These stresses often exceed initial design expectations and can significantly degrade

the mechanical performance, fatigue resistance, and dimensional stability of welded components. Traditional analytical methods are often insufficient to accurately capture the complex thermal cycles and stress distributions that develop during welding, especially in high-precision applications.

Induced stresses particularly residual stresses arise due to the rapid heating and cooling cycles inherent in welding. These thermal gradients create localized plastic deformation, leading to permanent stresses within the material even after it has cooled. The consequences of such stress fields are numerous and critical.

One major issue is distortion and warping, which occur when differential thermal expansion and contraction across the weldment generate uneven shrinkage forces. This leads to bending, twisting, or misalignment of the welded structure, compromising dimensional tolerances and requiring costly corrective actions. Warping, a form of distortion, can especially affect flat components, resulting in poor assembly fit and reduced structural functionality (Kou, 2003; Messler, 2008).

Another concern is cracking, including both hot and cold cracks. Hot cracks typically develop during solidification when the weld metal is still partially molten and subject to tensile stresses or segregation of low-melting constituents. Cold cracks, on the other hand, form after the weld has cooled and are often caused by residual stresses, hydrogen embrittlement, or the formation of brittle microstructures such as martensite. Both types of cracking compromise the mechanical integrity of welded joints and may necessitate expensive repairs or lead to premature failure (*Kou, 2003*).

Furthermore, residual stresses significantly contribute to reduced fatigue life. Welded components are particularly vulnerable to fatigue failure due to stress concentrations at weld toes, notches, or

embedded defects such as porosity and inclusions. These sites become initiation points for fatigue cracks, which propagate under cyclic loading and shorten the service life of critical structures like bridges, pipelines, pressure vessels, and aircraft components (Lindgren, 2001; Kou, 2003).

Applying SIMUFACT to simulate the actual maximum stress in tig weldment will therefore aid in mitigating against structural failure resulting from stress concentration in welded joints.

1.3 AIM AND OBJECTIVES

The aim of this project is to develop a robust predictive model, leveraging the SIMUFACT software, to understand and control the actual maximum stress induced in Tungsten Inert Gas (TIG) weldments

To achieve this aim, the following specific objectives will be pursued:

I. Conduct a review of recent relevant existing literature on the application of Artificial Neural Networks in predicting the mechanical properties in TIG welded joints

II. Identify necessary TIG welding process (input) parameters and their range of values from previous studies.

III. To generate a robust experimental matrix using a suitable design expert component.

IV. Conduct TIG welding experiments on mild steel coupons and record the actual maximum stress values in the experimental samples.

V. Simulate the experimental result using SIMUFACT.

VI. carry out comparative analysis on the experimental and SIMUFACT result.

VII. ascertain their degree of correlation

1.4 SCOPE OF STUDY

The scope of this study is limited to the simulation of the actual maximum stress in a tig weldment using SIMUFACT by studying the effect of current,voltage and gasflowrate on stress-concentration in tig weldment stress concentration factors.

1.5 SIGNIFICANCE OF THE STUDY

This study focuses on the use of SIMUFACT simulations to analyze the maximum stress experienced in TIG weldments. The research will examine how various parameters such as welding speed, heat input, and material properties affect the stress distribution within the weldment. TIG welding is critical for manufacturing safety-sensitive components in industries such as nuclear, aerospace, and chemical engineering. Residual stresses are a major contributor to in-service failures; however, experimental techniques to measure these stresses, such as hole-drilling and neutron diffraction, are expensive and offer limited resolution (Deng, 2018; Kumar, 2020).

In contrast, SIMUFACT simulation provides a cost-effective and reliable alternative. It enables the prediction of stress hotspots that are difficult to access with traditional sensors, allows for optimization of welding parameters to reduce distortion and cracking, and can extend the service life of welded structures (Pandey *et al.*, 2021).

This study aims to bridge the gap between the accuracy of simulation tools and the reliability needed for industrial applications, thus advancing design protocols for high-performance weldments.

CHAPTER TWO

LITERATURE REVIEW

2.1 Welding process: Concept of Welding

Welding is a fundamental fabrication technique used to permanently join metal components through the application of heat, pressure, or a combination of both, with or without the use of filler material (Deng *et al.,* 2021). The goal is to achieve a metallurgical bond at the interface, enabling the joined structure to function as a single, continuous piece.

In modern engineering, welding is favored for its high strength, durability, and efficiency, especially in applications where reliability is critical, such as automotive, aerospace, shipbuilding, and structural steel fabrication (Zhang *et al*., 2019). During welding, localized heating causes melting of the base materials, which upon solidification, forms a solid joint. However, this thermal cycle often introduces residual stresses, distortion, and changes in microstructure, which can affect the performance and lifespan of the welded component (Huang *et al*., 2020).

Welding remains one of the most economical and versatile joining methods, and its continued development is essential for advancing manufacturing efficiency and structural integrity.

2.2 TYPES OF WELDING

Welding is a core process in fabrication that involves the permanent joining of materials, typically metals, by applying heat, pressure, or both. Over the years, various welding techniques have been developed to suit different materials, thicknesses, and applications. These welding types are typically classified based on their heat source and method of operation.

The major types of welding include:

2.2.1. Arc Welding

Arc welding uses an electric arc between an electrode and the base metal to generate the heat required for melting and joining the materials. It is widely applied due to its versatility, cost-effectiveness, and ability to weld a variety of metals and thicknesses. (Deng *et al*., 2021)

2.2.2 Gas Welding

Gas welding, most notably Oxy-Acetylene Welding (OAW), utilizes the combustion of oxygen and acetylene to generate a high-temperature flame for welding. Though less commonly used today in structural fabrication, it is still popular for repairs, brazing, and thin-sheet welding (Kalpakji and Schmid, 2014*)*.

2.2.3 Resistance Welding

This type uses pressure and electric current to generate heat at the interface of the materials being joined. It includes methods such as spot welding, seam welding, and projection welding, widely used in automotive and sheet metal industries for their speed and automation compatibility (Li and Guo, 2022).

2.2.4 Laser Beam Welding (LBW) and Electron Beam Welding (EBW)

Both processes use focused energy beams laser or electron to achieve deep, narrow, high-precision welds. These methods are particularly suited for high-value components in aerospace, defense, and electronics industries. They offer excellent control but require specialized, costly equipment (Zhou *et al*., 2023).

2.2.5 Solid-State Welding

Unlike fusion welding, solid-state welding does not involve melting the base materials. Instead, it joins materials through pressure, sometimes with heat, at temperatures below the melting point.

Types include friction stir welding (FSW), diffusion bonding, and ultrasonic welding. These techniques are beneficial for joining dissimilar or heat-sensitive materials (Huang *et al*., 2020).

The selection of an appropriate welding type depends on several factors such as material properties, desired joint strength, dimensional tolerances, and economic considerations. TIG welding, a type of arc welding, is the focus of this study due to its suitability for precision welds and stress-ensitive applications.

2.3 Categories of welding

Welding can be categorized into three main groups based on how materials are joined: fusion welding, pressure (solid-state) welding, and brazing and soldering. These categories help guide the selection of suitable joining processes for different materials and applications.

2.3.1 Fusion Welding

Fusion welding joins materials by locally melting the base metals so they coalesce upon cooling. Examples include Gas Tungsten Arc Welding (GTAW or TIG), Gas Metal Arc Welding (GMAW or MIG), and Shielded Metal Arc Welding (SMAW). These methods form a metallurgical bond by melting both the electrode (if consumable) and the workpieces in the weld pool, providing strong joints suitable for a wide range of thicknesses and metals.

Fusion welding processes offer flexibility and broad industrial use, but typically involve higher heat input, which can lead to distortion, residual stress, and microstructural alterations in the heat-affected zone.

2.3.2 Pressure Welding (Solid-State Welding)

Pressure welding joins materials without melting the base metals; instead, it relies on heat generated by pressure or friction to create a bond in the solid state. Prominent methods include:

i. Friction Welding (FRW): Workpieces are brought into contact under pressure while one piece rotates to generate frictional heat. This causes plastic deformation and forging of the joint area (e.g. inertia friction welding, rotary friction welding).

ii. Friction Stir Welding (FSW): A non-consumable rotating tool traverses along the joint, mechanically stirring and forging the material below its melting point. This process produces high-quality welds with minimal distortion and narrow heat-affected zones, ideal for aluminum, copper, and other alloys.

These solid-state methods significantly reduce defects such as porosity and residual stresses compared to fusion welding, producing stronger joints in many applications.

2.3.3 Brazing and Soldering

These joining processes involve a filler metal with a melting point below that of the base materials. Unlike fusion welding, brazing and soldering do not involve melting the parent metals:

i. Brazing: The filler metal melts and flows by capillary action into the joint between closely fitted parts, generating a strong bond upon cooling. The base metal remains solid throughout, minimizing distortion and preserving the original microstructure

ii. Soldering: Occurs at even lower temperatures (typically below 400 °C for soft solders), usually used for electronics and delicate applications. The joints formed are weaker than those of brazing or welding but sufficient for low-stress environments

Brazing offers advantages in joining dissimilar materials and providing clean, tight joints without fusion. However, it generally requires higher cleanliness, precise fit, and yields joints of lower mechanical strength compared to welded joints.

2.4 Tig Welding

Tungsten Inert Gas (TIG) welding, formally known as Gas Tungsten Arc Welding (GTAW), is a highly precise fusion welding process that employs a non-consumable tungsten electrode to produce the arc needed to melt and join metals. The weld zone is protected from atmospheric contamination using an inert shielding gas, most commonly argon, or a mixture of argon and helium, to prevent the absorption of oxygen, nitrogen, and hydrogen into the molten pool, which could otherwise lead to weld defects (Huang *et al.*, 2020).

Unlike many other welding processes that rely on consumable electrodes or flux materials, TIG welding allows for the independent control of heat and filler metal addition. The filler rod if used is manually fed into the weld pool, giving the welder greater control over bead shape and penetration. This makes TIG welding especially suitable for delicate operations, such as welding thin-gauge metals, dissimilar alloys, and applications requiring aesthetically clean and smooth weld finishes.

TIG welding is widely regarded for its ability to produce high-integrity, defect-free welds with minimal spatter and excellent mechanical properties. It is extensively used in aerospace, nuclear, automotive, petrochemical, and medical device industries, where weld precision and reliability are critical. The process is particularly advantageous when welding non-ferrous metals like aluminum, magnesium, and titanium, which are difficult to weld using conventional arc welding methods due to their thermal properties and oxidation tendencies (Zhang *et al*., 2019).

Despite its many strengths, TIG welding does come with limitations. The process is generally slower than other arc welding methods, such as MIG or SMAW, and requires significant operator skill to manage heat input, maintain arc stability, and control filler deposition. Furthermore, the equipment setup is relatively more complex and expensive, especially when dealing with AC current for aluminum welding or when using pulse-current control features.

Nevertheless, the precision, control, and weld quality offered by TIG welding make it an indispensable method for applications where weld performance, aesthetics, and structural integrity are non-negotiable. As industries continue to demand higher standards in welded components, TIG welding remains a cornerstone of high-performance fabrication technologies.

2.4.1 Advantages Of Tig Welding

i. Produces high-purity, clean welds with minimal defects.

ii. Excellent control over heat input and arc.

iii. Suitable for thin materials and non-ferrous metals.

iv. Minimal post-weld cleaning required (Zhou *et al*., 2023).

2.4.2 Disadvantages Of Tig Welding

i. Requires high operator skill level.

ii. Slower welding speed compared to other arc methods.

iii. Equipment is more expensive and complex.

iv. Limited in welding thick materials economically (*Li and Guo, 2022*).

2.4.3 TIG Welding Process Parameters

The effectiveness and quality of TIG welding are highly influenced by several critical process parameters, each of which plays a significant role in the weld characteristics and structural integrity of the joint:

i. Current and Voltage: TIG welding uses either direct current (DC) for materials like stainless steel or alternating current (AC) for metals such as aluminum and magnesium. These parameters directly influence arc behavior, heat input, and penetration depth.

ii. Shielding Gas Flow Rate: The flow rate of inert gases, primarily argon or a mixture of argon and helium, determines the stability of the welding arc and protects the molten weld pool from atmospheric gases. Inadequate flow can result in porosity, oxidation, or arc instability.

iii. Electrode Type and Size: The choice of tungsten electrode (e.g., pure tungsten, thoriated, or ceriated) and its diameter influence the concentration of heat and arc ignition. Smaller electrodes are used for low current and precise welds, while larger ones handle higher currents.

iv. Travel Speed and Torch Angle: The speed at which the torch moves and the angle of inclination affect weld bead appearance, penetration, and potential defects. Too fast a speed may lead to insufficient fusion, while too slow can cause overheating and distortion.

v. Filler Material: Selection of a compatible filler rod based on the base metal and joint design ensures mechanical strength and chemical consistency of the weld. Mismatched filler materials can lead to weak or brittle welds.

Optimizing these parameters is crucial to ensure high weld quality, reduce the occurrence of defects such as undercuts, porosity, and incomplete fusion, and to limit the extent of the heat-affected zone (HAZ**)** (Deng *et al*., 2021).

2.5 Induced Stress and Its Effect in Weldment

Welding processes inherently involve non-uniform heating and cooling, which leads to the development of induced stresses within the welded structure. As the weld zone expands and contracts at different rates compared to surrounding base metal, internal stress fields are created. These stresses can be tensile or compressive, and in many cases, remain in the structure long after the welding operation is completed.

The presence of induced stress is critical because it can lead to distortion, cracking, fatigue failure, or even stress corrosion, especially under service loading conditions. Managing or mitigating these stresses is essential to ensure long-term durability, dimensional accuracy, and mechanical integrity of the welded component.

2.5.1 Categories of Stress

Induced stresses in welding can generally be categorized into the following major types:

i. Thermal Stress: Caused by rapid thermal expansion and contraction during the heating and cooling phases of welding. Localized heat inputs create significant temperature gradients, leading to internal strains.

ii. Residual Stress: These are locked-in stresses that remain in the material after it has cooled to ambient temperature. Residual stresses may not show immediate effects but can significantly affect fatigue life, crack propagation, and dimensional stability over time.

iii. Mechanical Stress: Generated by external forces or service loads applied to the weldment during its operational life. When combined with residual stresses, they can initiate failure modes if not properly accounted for (*Withers and Bhadeshia, 2001*).

2.5.2 Effects Of Induced Stress On Welded Structure

Induced stress can:

i. Lead to crack initiation and propagation.

ii. Reduce fatigue life of the component.

iii. Cause distortion and warping.

iv. Increase susceptibility to stress corrosion cracking **(***Huang et al., 2020***).**

2.5.3 Conventional Method For Mitigating Against Stress In Weldment

Residual and induced stresses in welded structures can severely compromise the structural performance, fatigue resistance, and dimensional accuracy of components. To address these challenges, several conventional stress-relief techniques have been developed and widely adopted in welding practices to either eliminate or reduce harmful tensile stresses and distortions in weldments.

Key traditional methods include:

i. Post-Weld Heat Treatment (PWHT)**:**

PWHT involves controlled heating of a welded component to a specified temperature, holding it for a predetermined time, and then cooling it gradually. This process allows internal stresses to

redistribute more evenly through plastic deformation and creep relaxation. It is especially useful in pressure vessels, pipelines, and structural steel components where weld integrity is critical.

ii. Peening:

Mechanical peening (e.g., shot peening or hammer peening) is used to impart compressive stress on the surface of a weld, counteracting tensile residual stresses generated during welding. This technique enhances fatigue life by making crack initiation less likely at the surface level.

iii. Weld Sequencing and Clamping:

Strategic weld sequencing planning the order and direction of welding passes helps balance stress accumulation and reduce distortion. In conjunction, clamping and fixturing are employed to restrain movement and maintain dimensional control throughout the welding process.

iv. Thermal Tensioning**:**

This method involves selectively heating specific zones around the weld to counteract thermal contractions, thereby reducing the formation of tensile residual stresses in the final structure (Zhang *et al*., 2019).

These methods, though traditional, remain highly effective in managing stress in welded joints. They are often used in combination depending on material type, component geometry, and service conditions, and continue to form the foundation for more advanced, simulation-assisted stress mitigation strategies in modern manufacturing.

2.6 Actual Maximum Stress

The actual maximum stress in a welded joint is defined as the highest level of stress, whether residual (left over from the welding process) or operational (applied during the component's

service), that exists within or around the weld zone. This critical stress point often governs the structural performance, failure behavior, and fatigue life of welded components.

During welding, extreme localized heating followed by rapid cooling introduces complex thermal gradients. These lead to uneven expansion and contraction of the material, thereby generating residual stresses. In addition to those locked-in stresses, welded components are also exposed to external operational loads during service such as pressure, vibration, bending, or thermal cycles that can amplify the total stress experienced by the structure.

Identifying the actual maximum stress is of paramount importance for several reasons:

i. It helps in determining the true load-bearing capacity of the welded joint.

ii. It enables accurate life prediction and crack initiation analysis, particularly under cyclic loading conditions.

iii. It allows engineers to apply appropriate design safety factors or stress-relief techniques to prevent structural failure.

Failure to accurately assess the actual maximum stress may lead to premature failures, especially in high-pressure or safety-critical applications such as pressure vessels, bridges, pipelines, and aircraft structures. Furthermore, the complex stress distribution near the heat-affected zone (HAZ) and weld toe often makes visual or manual assessment inadequate, necessitating the use of advanced computational or experimental stress analysis techniques.

Modern tools such as finite element simulation and X-ray diffraction now make it possible to capture these peak stress values with high accuracy and resolution *(*Deng *et al*., 2021). These

methods have proven instrumental in identifying critical stress zones that may not be visible through traditional inspection techniques.

2.6.1 Causes of Actual Maximum Stress in Welded Structures

Actual maximum stress arises due to a combination of the following factors:

i. Welding Residual Stress: Caused by non-uniform thermal cycles during welding, resulting in high tensile stresses.
ii. Stress Concentration at Weld Geometry: Weld toes, undercuts, and discontinuities often create regions of sharp gradients in stress.
iii. Material Inhomogeneity: The weld metal, base metal, and HAZ often possess differing mechanical properties, contributing to stress mismatches.
iv. External Loading Conditions: In-service loads combined with residual stresses may amplify local stress states.
v. Thermal Expansion and Shrinkage: The differential expansion and contraction of welded materials leads to stress accumulation, particularly in constrained joints (Masubuchi, 1980).

2.6.2 Methods for Measuring Actual Stress

Measuring the actual stress in a welded structure requires both experimental and computational techniques. These methods vary in their accuracy, depth of penetration, destructiveness, and cost:

i. X-ray Diffraction (XRD) and Neutron Diffraction: These are non-destructive techniques widely used to measure residual stress by analyzing lattice strain in crystalline materials. While XRD is

ideal for surface-level stress analysis, neutron diffraction can penetrate deeper into materials, providing subsurface stress profiles (Withers and Bhadeshia, 2001).

ii. Strain Gauges: These are electrical sensors attached to the surface of components to measure deformation caused by applied or residual stress. Though limited to surface measurements, they are highly useful in real-time operational stress monitoring.

iii. Hole-Drilling Method: This is a semi-destructive technique used for measuring residual stresses near the surface. A small hole is drilled into the component, and the resulting deformation is analyzed using strain gauges to back-calculate the stress distribution.

Iv. Analytical Methods:

Analytical approaches often use closed-form equations and fracture mechanics principles to estimate the actual maximum stress. For example:

a. Stress concentration factors (SCFs) from standard geometries (fillet welds) help calculate amplified stress based on notch effects.
b. Nominal stress method combined with SCFs:

   $\sigma max = Kt \cdot \sigma nominal$

   Where Kt is the theoretical stress concentration factor.

2.6.3 Application of SIMUFACT in simulating welding process.

SIMUFACT Welding is a specialized software used to simulate and analyze various welding processes, including Tungsten Inert Gas (TIG)**,** MIG, and resistance welding. It helps engineers predict how heat and stress develop in a welded structure during and after welding.

The software uses temperature-dependent material properties and process parameters such as current, voltage, welding speed, and gas flow rate to model the real welding environment. It provides visual and numerical results showing temperature distribution**,** residual stress**,** distortion**,** and deformation in the weldment (Hexagon, 2023; Kou, 2021).

By applying SIMUFACT, researchers can optimize welding parameters, reduce defects, and minimize the number of experimental trials required. This makes it a powerful and cost-effective tool for predicting actual maximum stress and improving the quality of welded joints (Li and Zhang, 2020).

2.7 Stress Simulation Techniques

Stress simulation techniques, particularly those based on numerical modeling, play a crucial role in modern welding analysis. These techniques allow engineers to simulate real-world operating conditions and predict the mechanical response of welded structures before physical fabrication.

Simulations help visualize:

i. Stress distribution across the weldment,

ii. Locations of hot spots and potential crack initiation sites,

iii. Deformation patterns due to thermal loading and mechanical stress.

Advanced simulation models can replicate welding thermal cycles, material transformations, heat-affected zone evolution, and stress-strain interactions. This predictive capability enables better design optimization, welding process control, and failure prevention (Deng *et al.*, 2021; Zhou *et al*., 2023).

By incorporating material properties, boundary conditions, and welding parameters, these techniques provide insight that is often difficult or impossible to obtain experimentally.

2.8 SIMUFACT SIMULATION

SIMUFACT Welding is a process-oriented simulation software developed by Hexagon Manufacturing Intelligence, designed for the analysis of welding and joining processes. The software predicts critical welding phenomena such as heat transfer, distortion, and residual stress in welded structures by utilizing material-specific thermal and mechanical data (Görög et al., 2018; Szwed *et al*., 2020).

2.8.1 Welding Parameters and Boundary Conditions

The welding parameters applied in the simulation are consistent with experimental settings: current (170–190 A), voltage (22–25 V), and gas flow rate (14–17 L/min). The plates were assumed to be at room temperature (25°C) before welding. Mechanical constraints were applied to simulate clamping, while convection and radiation losses were considered at the free surfaces (Kou, 2021).

2.9 Safety Procedures

Safety in welding is critical due to the risks of high temperatures, UV radiation, toxic fumes, and electric shock. Standard safety practices include:

I. Wearing personal protective equipment (PPE): gloves, helmets, aprons, and eye protection.

II. Ensuring adequate ventilation to avoid fume inhalation.

III. Maintaining equipment integrity and grounding to prevent electric hazards.

IV. Following OSHA or local safety regulations (AWS, 2020; Kalpakjian andand Schmid, 2014).

CHAPTER 3

METHODOLOGY

In the previous chapter we made a perspective sketch of the various relevant research works surrounding the present research study. In this chapter we shall explain the research strategy to be employed to obtain and analyze data for the study. The methodological steps are as follows;

i. Identification of input parameters range

ii. Samples and sampling technique

iii. Experimental data collection

iv. Experimental data analysis

3.1 Identification of Input Parameters Range

The key parameters to be considered in this work are welding current (A), welding voltage (V), Gas FlowRate (L/Min). The range of the process parameters to be used were obtained from relevant recent literature is tabulated below.

Table 3.1: Process parameters and their level

AMETERS	**NITS**	**SYMBOL**	**MINIMUM VALUE**	**AXIMUM UE**
ing Current			0	0
ing Voltage				
low Rate				

The following materials and equipment would be used to effectively and successfully carry out this research study: mild steel plates, power hacksaw, a TIG welding machine, argon gas and a Finite element method.

3.2 Samples and sampling technique

The weld samples will be made from mild steel plates and cut to size using hack saw, edges grinded, surface polished with emery paper and the joint welded. A tungsten inert gas welding equipment will be used to carry out the welding process on the mild steel plates. The TIG welding process will use a shielding gas to protect the weld specimen from atmospheric interaction, 100% pure Argon gas will be used for this research study. The TIG welding machine alongside the argon gas is as shown in Plate 3.1.

Fig 1: TIG welding equipment with argon gas cylinder

Fig 2: Argon gas cylinder

Universal Stress Testing Machine

A Universal Stress Testing Machine (commonly known as a Universal TestingMachine, or UTM) is a multi-purpose material testing instrument used to evaluate the mechanical properties of materials under various types of loading conditions, such as tension, compression, bending, and shear. It is termed “universal” because it can perform a wide range of standardised mechanical tests on diverse materials including metals, plastics, ceramics, polymers, and composites (Budynas and Nisbett, 2015).

Fig 3 Universal stress testing machine

3.3 Experimental Data Collection

The input parameters (Current, Voltage and Gas flow rate) will be used as factors for the design matrix. The central composite design (CCD) interphase of VERSION 13.05 Design Expert will be used to develop a statistical design of experiment. The CCD matrix utilizing the three input parameter generatedanexperimental design matrix having six (6) center points (no), six (6) axial points (2n) and eight (8) factorial points (2 n) which when imputed into Equation 3.1 resulted in twenty (20) experimental runs. The CCDmatrix is presented in Table 3.2. The total number of experimental runs as generated by the CCDis given as:

$$N = 2^n + n_o + 2n \quad (3.1)$$

where; N: is the number of experimental runs based on CCD, 2^n : is the number of factorial points, no: is the number of center points, 2n: is the number of axial points and n: is the number of variables. Table 3.2shows the experimental matrix generated by the CCD.

Table 3.2 Central Composite Design (CCD) Experimental Matrix Factors

Run	Factor 1	Factor 2	Factor 3
	A: Current (Amp)	B: Voltage (Volt)	C: Gas Flow Rate (lit/min)
1	170	22	14
2	170	23	15
3	190	24	16
4	170	25	17
5	180	22	15
6	170	23	16

7	**180**	**24**	**17**
8	**160**	**25**	**14**
9	**180**	**22**	**16**
10	**160**	**23**	**17**
11	**160**	**24**	**14**
12	**160**	**25**	**15**
13	**180**	**22**	**17**
14	**170**	**23**	**14**
15	**170**	**24**	**15**
16	**170**	**25**	**16**
17	**170**	**25**	**17**
18	**170**	**24**	**14**
19	**160**	**23**	**15**
20	**170**	**22**	**16**

3.4 Experimental Data Analysis

In this study, the Finite Element Method (FEM) is used as a numerical tool to analyze stress distribution in TIG-welded joints. The simulation provides virtual experimental data that replicates real-world welding conditions, helping to determine stress concentration factors (SCF) and identify critical stress zones.

The analysis begins with creating a CAD model of the weldment, followed by meshing, applying boundary conditions, and assigning material properties. Loads simulating thermal and mechanical effects from welding are applied. The simulation then calculates stress and strain distributions across the model.

From the results, the maximum stress near the weld toe and the nominal stress in the base material are used to compute the SCF using:

$K_t = \sigma_{max} / \sigma_{nom}$

This method allows for detailed, cost-effective analysis of weld performance, aiding in failure prediction and design optimization.

CHAPTER FOUR

RESULTS AND DISCUSSION

This chapter presents the results obtained from both the experimental tests and the SIMUFACT simulations conducted using SIMUFACT Welding 2024. The study aims to predict and validate the actual maximum stress developed in Tungsten Inert Gas (TIG) welded joints under varying process parameters. The results are organized into three parts:

(i) presentation of actual experimental data,

(ii) simulation of the welding process using SIMUFACT

(iii) Presentation of SIMUFACT result

(iv) Comparison between the actual experimental result and the SIMUFACT result

4.1 Presentation of The Experimental Results

The experimental phase involved TIG welding of low carbon steel plates (S235) under systematically varied process parameters—welding current, voltage, and shielding gas flow rate. The welded specimens were mechanically tested to determine the maximum stress sustained by each weldment.

Table 4.1: Experimental Results for TIG Welded Samples

Run	Current (A)	Voltage (V)	Gas Flow (L/min)	Experimental Maximum Stress (MPa)
1	170	22	14	355.04
2	170	23	15	354.97
3	190	24	16	311.28
4	170	25	17	319.7
5	180	22	15	354.44
6	170	23	16	353.97
7	180	24	17	316.02
8	160	25	14	353.26
9	180	22	16	352.85
10	160	23	17	357.3
11	160	24	14	349.07
12	160	25	15	355.52
13	180	22	17	355.85
14	170	23	14	355.75
15	170	24	15	344.11
16	170	25	16	317.48
17	170	25	17	316.46
18	170	24	14	345.6
19	160	23	15	357.14

20	170	22	16	355.73

Observations shows that the ranges of welding current is from 160A-190A, voltage is from 22V-25V and gas flow rate is from 14L/min – 17L/min. The experimental results show that the maximum stress values ranged between 311 MPa and 357 MPa, with the highest value (357.30 MPa) recorded at a relatively low current (160 A) and voltage (23 V). This suggests that higher heat input reduces the cooling rate, thereby lowering residual stress, whereas lower currents produce sharper thermal gradients and higher stress accumulation.

4.2 Simulation of The Welding Process Using SIMUFACT

The experimental welding process parameters were replicated in SIMUFACT Welding 2024, using a thermomechanical arc welding process model with double-ellipsoidal heat source distribution. The simulated model included two S235-SPM-sw mild steel plates joined in a butt joint configuration, with clamping at both ends and a total welding time of 22 seconds.

The material properties, boundary conditions, and solver settings were as follows:

i. Process type: Arc welding (manual)
ii. Ambient temperature: 20 °C
iii. Welding velocity: 5 mm/s
iv. Heat input (net): 6732 J/cm
v. Efficiency: 0.9
vi. Solver: MUMPS parallel direct solver (4 processors)
vii. Total time: 22 s (0–22 s)
viii. Elements: 3,280 solid elements and 5,262 surface elements

The simulated low carbon steel S256 plates as developed by SIMUFACT is as shown in Figure 4.1

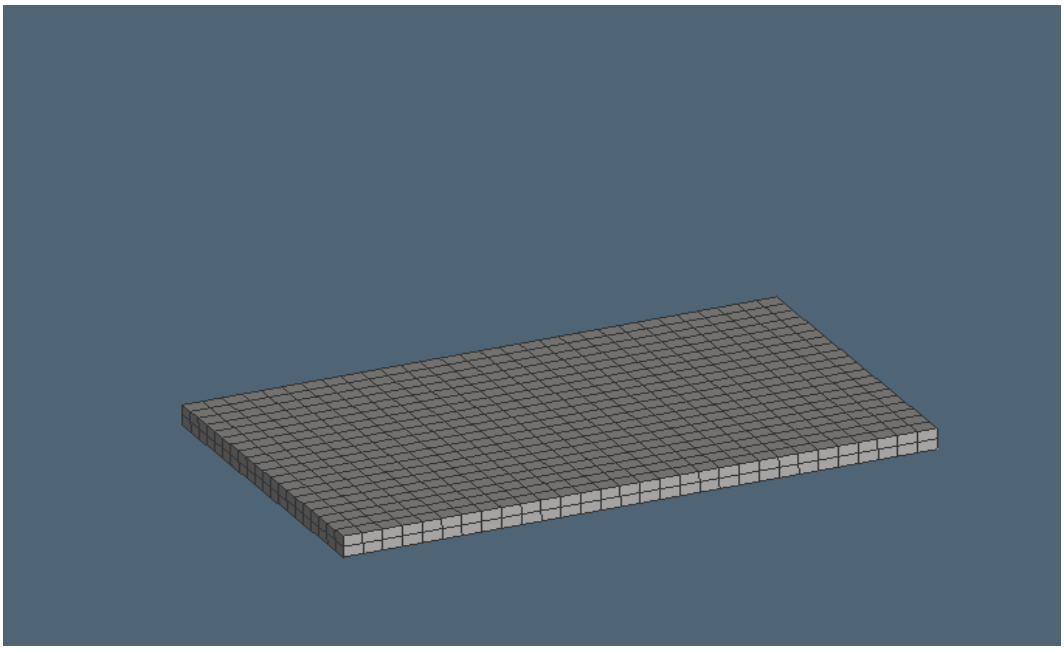

Fig.4.1 TWO S235-SPM-SW MILD STEEL PLATES

Time intervals of trajectories

The time trajectory ranges from 00s to 22s from start time to end time

Process report

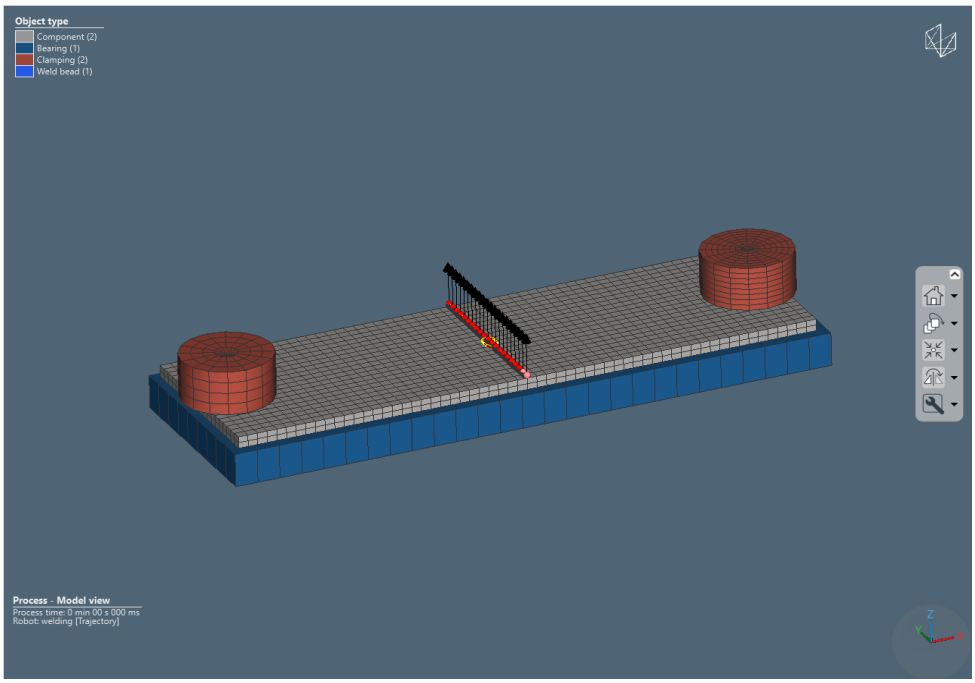

Fig. 4.3 COMPONENT, BEARING, CLAMPING AND WELD BEAD

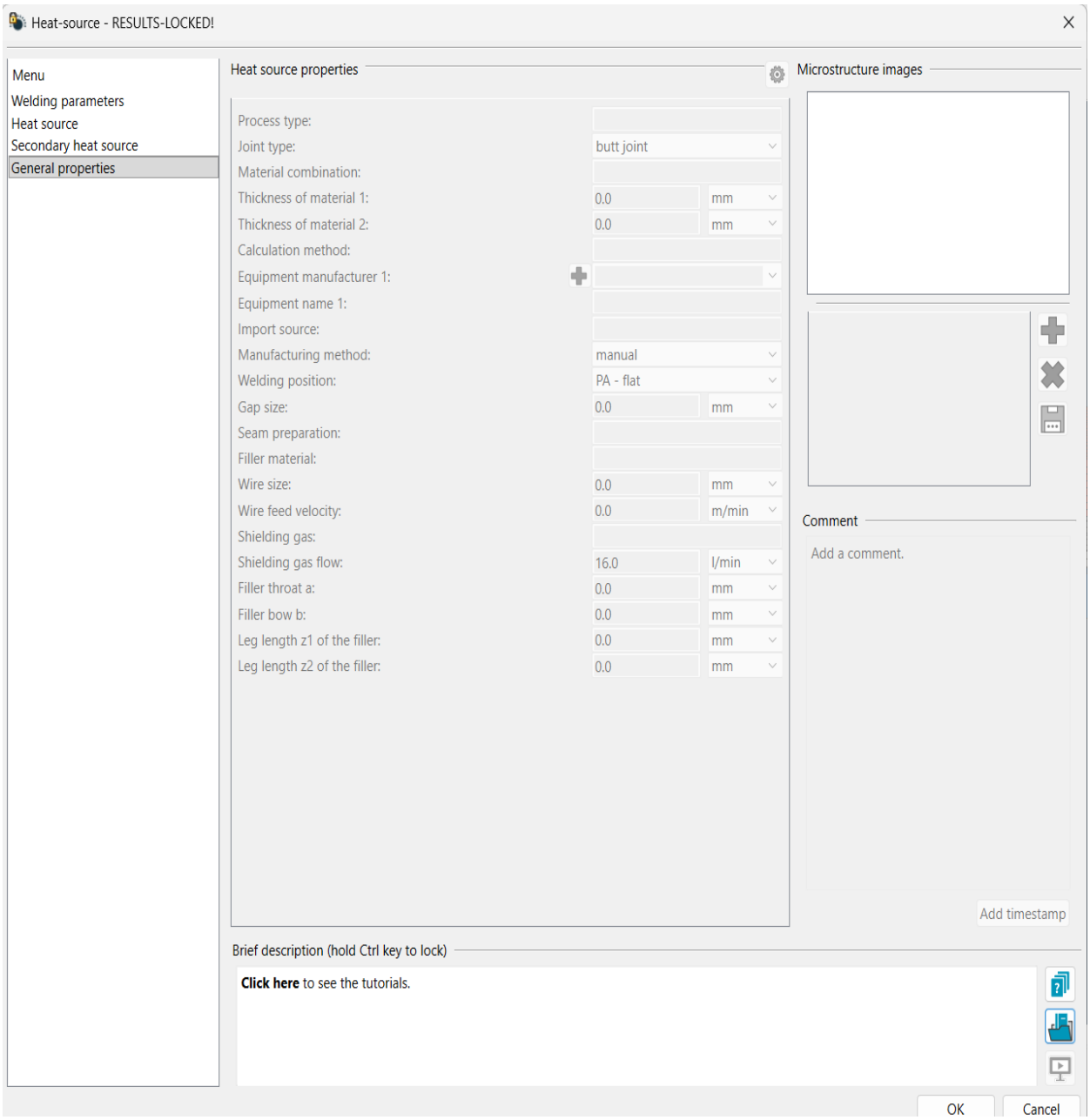

Fig.4.4 input parameters of the shielding gas flow rate and weld type

Process parameters

a) Process type: Arc welding

b) Shrinkage active: no

c) Single-shot solution: no

d) Solution: Thermomechanical

e) Symmetry plane: not available

f) Ambient temperature: 20.0 °C

Process Parameters Explanation

In carrying out the simulation analysis, several process parameters were defined to ensure accurate and efficient computation of the forming operation. The solver type selected was MUMPS (Multifrontal Massively Parallel Sparse) Parallel Direct, a highly efficient numerical solver capable of handling large and complex finite element models. It employs a parallel direct matrix solution method that allows the program to perform simultaneous calculations across multiple processors, thereby improving computational speed and stability. To further enhance performance, multiprocessing with four processors was activated, allowing the simulation to utilize four CPU cores for faster data processing and reduced solution time.

The phase transformation option was not used in this analysis. This means that the simulation focused solely on the mechanical deformation behavior of the material without accounting for any temperature-induced changes in the material's microstructure. This approach is suitable when the forming process occurs under conditions where phase changes are negligible or not of interest. Additionally, high-end contact separation with prevention of chattering was employed. This parameter improves the accuracy of surface contact interactions between the die and the workpiece, ensuring that contact and separation occur smoothly. The prevention of chattering helps to avoid numerical

instabilities and oscillations that can occur when surfaces repeatedly make and lose contact, leading to more realistic simulation results. Finally, the domain decomposition was set to one domain, meaning that the model was solved as a single continuous computational region. This simplifies the numerical process and ensures consistent convergence of results, particularly when dealing with moderately sized models that do not require extensive parallel subdivision.

Analysis Time and Model Refinement Parameters Explanation

The analysis time in the simulation was defined with a start time of 0.0 seconds and an end time of 22.0 seconds, indicating that the entire forming or welding process was numerically observed over a 22-second duration. This range represents the total time interval in which deformation, heat transfer, and other process responses were computed. The time step calculation was set to fixed (automatic), meaning that the software automatically controlled the size of each time increment during computation. This ensures numerical stability and accuracy by adjusting the time step according to the process dynamics, especially during complex interactions such as contact or heat input phases.

For the result time steps, a cooling time of 5.0 seconds was applied. This setting enabled the simulation to capture the cooling behavior of the workpiece after the primary forming or heating operation. The inclusion of cooling time allows for a more realistic thermal response, as temperature gradients and residual stresses often develop during this stage.

The refinement parameters were set with a refinement level of 0, meaning that no additional mesh refinement was applied to the model. In SIMUFACT analysis, refinement refers to increasing the mesh density in regions of high stress or thermal gradients to obtain more accurate results. Since the refinement level was zero, the standard mesh resolution was

considered sufficient for the simulation's objectives. Additionally, the heat source area scaling factor was set to 1.2, which slightly expanded the effective area influenced by the applied heat source. This adjustment helps to better represent the actual heat distribution within the material during the simulated process.

The global unrefinement settings were configured with the type set to "none" and level set to 0, indicating that no automatic coarsening of the mesh occurred during the simulation. Unrefinement is typically used to reduce computational load by coarsening the mesh in regions where deformation or temperature change is minimal. However, by turning it off, the analysis maintained a consistent mesh density throughout the process, ensuring uniform accuracy. The "prevent unrefinement in contact area" option was also set to off, meaning that the mesh in contact regions was not restricted from adjustment, though no unrefinement occurred in this case.

Table 4.2 Loadcase times

Number	Start time [s]	Stop time [s]	Initial time step	Minimum time step	Maximum time step	Steps	Loadcase	Loadcase name
1	0.0	22.0	0.624856	1e-06	0.624856	36	Welding	welding_1

Components

In the simulation setup, two primary components were defined: *plate-mm* and *plate-mm-2*. Both components were assigned the same base material, S235-SPM-sw, which is a structural steel commonly used in welding and mechanical simulations due to its predictable mechanical behavior and weldability. The initial temperature for each component was set at 20.0°C, representing

ambient room temperature conditions prior to the application of thermal and mechanical loads. The geometric definitions of the components were identified as *plate-mm* and *plate-mm-2*, respectively, corresponding to the modeled weld plates in the simulation environment. Neither of the components was used as filler material, as indicated by the inactive filler setting. Furthermore, there were no result value transfers available at this stage, implying that no preliminary computational data were carried over from prior analyses. This configuration establishes the foundational parameters for the TIG weldment simulation, ensuring that both plates begin under identical initial conditions for accurate stress and thermal response comparison during the welding process. The SIMUFACT welding process was set in the following conditions.

i. In the welding simulation, several boundary and process conditions were defined to ensure realistic modeling of the TIG welding operation. The analysis was conducted over a total duration of 22.0 seconds, beginning at 0.0 seconds and ending at 22.0 seconds, representing the complete thermal and mechanical cycle of the welding process. A bearing geometry was included in the model to provide necessary support and constrain specific degrees of freedom during the simulation. However, the process did not incorporate any fixed geometries or fixed nodes, indicating that the plates were free to expand or contract under thermal loads within the constraints provided by the bearings and clamps.

ii. Two clamping conditions—identified as *Clamping* and *Clamping-2*—were applied at the start of the analysis to stabilize the plates throughout the welding process. Each clamp was assigned a spring stiffness of 1000.0 N/m and a holding force of 0.05 kN, ensuring controlled restraint without over-constraining the model. These parameters simulate the practical conditions used to secure workpieces during TIG welding operations, minimizing distortion while allowing limited thermal expansion.

iii. The simulation did not employ any local joints or virtual pins, confirming that no additional localized constraints or rotational joints were introduced in the setup. For the robotic welding operation, a standard robot model was utilized with an ambient temperature of 20.0°C, corresponding to room temperature conditions. The robot executed a single weld bead along a trajectory length of 110.0 mm, with the same total working time of 22.0 seconds. The welding trajectory and associated heat source parameters were predefined and controlled to ensure accurate simulation of heat input and weld pool development during the process.

iv. This configuration collectively represents a realistic setup for thermal–mechanical simulation in TIG welding using SIMUFACT Welding software, ensuring accurate prediction of induced stress, heat distribution, and deformation behavior across the weldment.

Table 4.3: Time summary

Order	Trajectory	Length	Start welding	End welding	Welding time	End time	Welding parameter	Welding filler
1	Trajectory	110.0 mm	0.0 s	22.0 s	22.0 s	22.0 s	Heat-source	Trajectory-weldbead

Geometrical and Material Properties Configuration for simulation

The simulation model comprised multiple geometrical components, including *plate-mm*, *plate-mm-2*, *bearing*, *clamping*, *clamping-2*, and *trajectory-weldbead*. Each of these geometries was defined to replicate the real TIG welding setup as accurately as possible. Both *plate-mm* and *plate-mm-2* were modeled in **millimeters**, with each surface mesh consisting of **1402 nodes** and **1400 elements**, while the corresponding volume model contained **1953 nodes** and **1200 elements**. These two plates represent the base materials joined during welding. The **bearing geometry**, modeled in **meters**, provided essential mechanical support, consisting of **560 nodes** and **558 elements** on its surface, with no volume model defined. Similarly, the **clamping geometries** (*clamping* and *clamping-2*) were used to restrain the plates during welding, having **368 nodes and 380 elements**, and **176 nodes and 188 elements**, respectively, in their surface models. The **trajectory-weld bead** geometry represented the path of the weld bead, modeled in **meters**, consisting of **1338 nodes** and **1336 elements** in its surface model, and **1665 nodes** with **880 elements** in its volume mesh. This geometric definition ensured adequate mesh refinement in critical regions such as the weld zone and heat-affected areas to capture temperature gradients and stress distributions effectively.

The base material, *S235-SPM-sw*, was generated from multiphase model data with an initial phase composition of **93% ferrite** and **7% pearlite**, neglecting transformation effects. The alloy composition was obtained from JMatPro and comprised approximately **0.15% C**, **0.4% Cu**, **98.29% Fe**, **1.1% Mn**, **0.01% N**, **0.02% P**, and **0.027% S**, with an **austenitization temperature of 1300°C** and a **cooling rate of 171.01°C/s**. The grain size corresponded to **ASTM 7.51**, and flow curves were calculated with an initial microstructure size of **30 microns**. The Poisson's ratio for this material was set to **0.3**, while its electrical properties were referenced from Wink and

Krätschmer (2012).

The filler material, *SG1-JMP-MPM-sw*, was similarly defined using JMatPro version 6.2. Its alloy composition included approximately **0.1% C**, **0.65% Si**, **1.1% Mn**, **0.15% Mo**, **0.15% Ni**, **0.15% Ti**, and **97.68% Fe**, with a corresponding **ASTM grain size of 11.71** and an **austenitization temperature of 1300°C**. The **cooling rate was 196.92°C/s**, and a **Poisson's ratio of 0.3** was adopted. These material definitions ensured accurate modeling of thermal conductivity, yield behavior, and phase response during the heating and cooling cycles of TIG welding.

The **welding trajectory** was globally oriented and consisted of **21 data points**, all of which were active during the simulation, representing a continuous weld path along the plate joint. The heat source was defined as a **conventional TIG welding model** with a **butt joint configuration** and a **flat (PA) welding position**, consistent with typical TIG welding setups. Although filler parameters such as wire size and feed velocity were not explicitly modeled, shielding gas flow was defined as **0.000266667 m³/s**, providing inert gas protection during the simulated process. The welding current and voltage were set to **170 A** and **22 V**, respectively, producing a **gross energy input of 7480 J/cm** and a **net energy input of 6732 J/cm** with an assumed **efficiency of 0.9**. The welding speed was maintained at **5.0 mm/s**, under a **transient specification mode** using indirect power control.

The heat source geometry parameters included a **front length of 2.89 mm**, a **rear length of 11.57 mm**, a **width of 3.99 mm**, and a **penetration depth of 8.30 mm**, representing the molten pool dimensions during welding. These parameters were scaled using a **heat front factor of 0.4** to simulate the Gaussian heat distribution typical of TIG arcs. Collectively, these inputs provided a comprehensive thermal–mechanical environment for the simulation, enabling accurate computation of temperature gradients, thermal stress development, and residual stress distribution

within the TIG-welded S235 steel plates. The individual simulation by SIMUFACT for the 20 runs are depicted as follows:

Run 1:

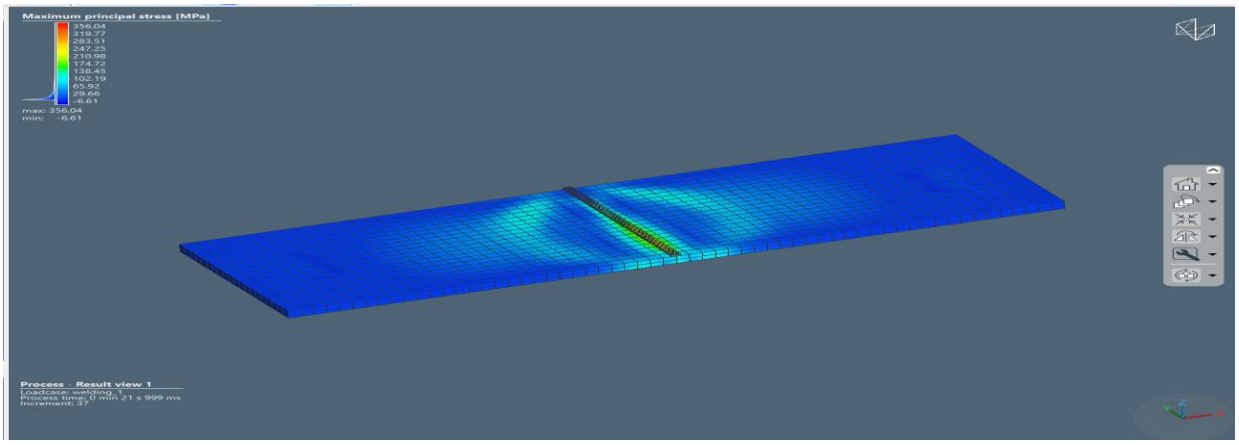

Fig.4.5 SIMUFACT simulation: RUN 1

The image shows the simulated maximum principal stress distribution in a TIG-welded joint, with peak stress (356.04 MPa) concentrated along the weld zone. The stress gradually decreases toward the base plates, indicating localized thermal and residual stress effects.

Run 2:

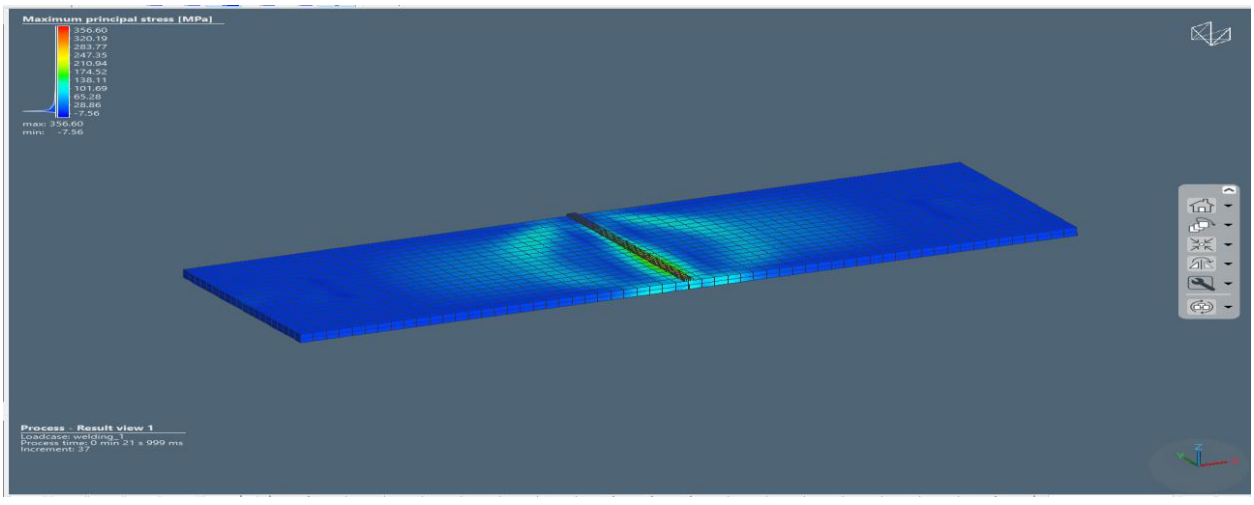

Fig.4.6 SIMUFACT simulation: RUN 2

The image shows the simulated maximum principal stress distribution in a TIG-welded joint, with peak stress (356.60 MPa) concentrated along the weld zone. The stress gradually decreases toward the base plates, indicating localized thermal and residual stress effects.

3rd Run

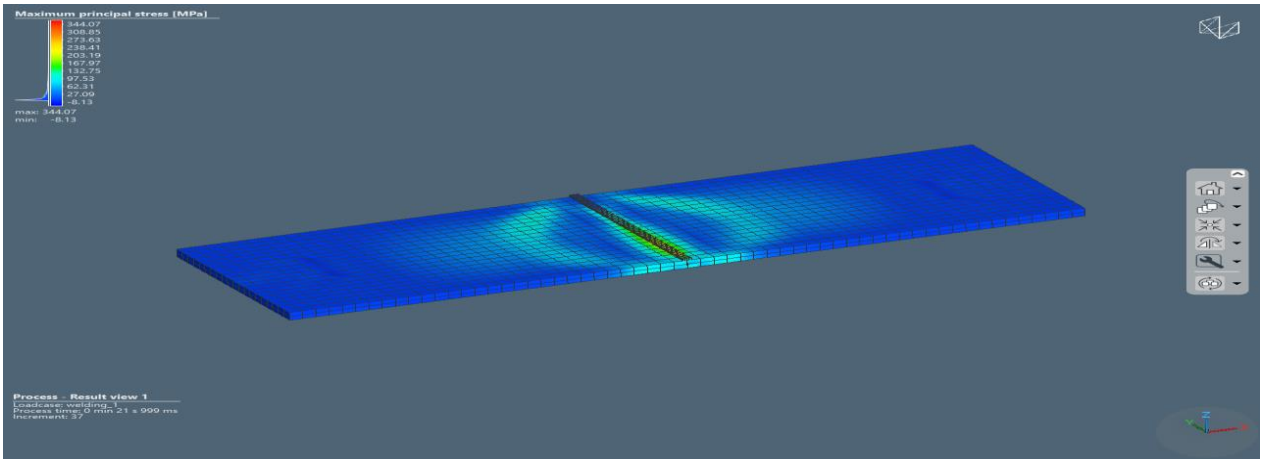

Fig.4.7 SIMUFACT simulation: RUN 3

The image shows the simulated maximum principal stress distribution in a TIG-welded joint, with peak stress (344.07 MPa) concentrated along the weld zone. The stress gradually decreases toward the base plates, indicating localized thermal and residual stress effects.

4th RUN

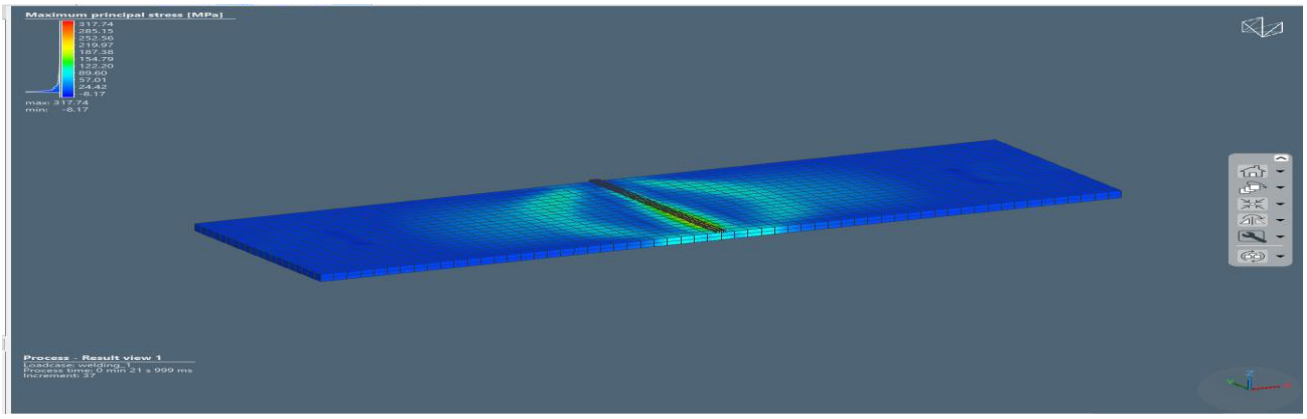

Fig.4.8 SIMUFACT simulation: RUN 4

The image shows the simulated maximum principal stress distribution in a TIG-welded joint, with peak stress (317.74 MPa) concentrated along the weld zone. The stress gradually decreases toward the base plates, indicating localized thermal and residual stress effects.

5TH RUN

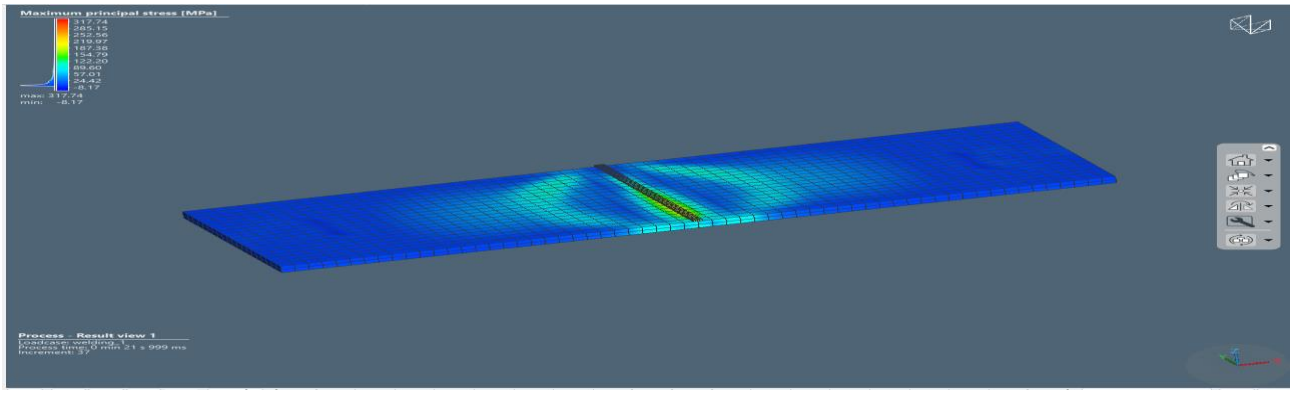

Fig.4.9 SIMUFACT simulation: RUN 5

The image shows the simulated maximum principal stress distribution in a TIG-welded joint, with peak stress (317.74 MPa) concentrated along the weld zone. The stress gradually decreases toward the base plates, indicating localized thermal and residual stress effects.

6TH RUN

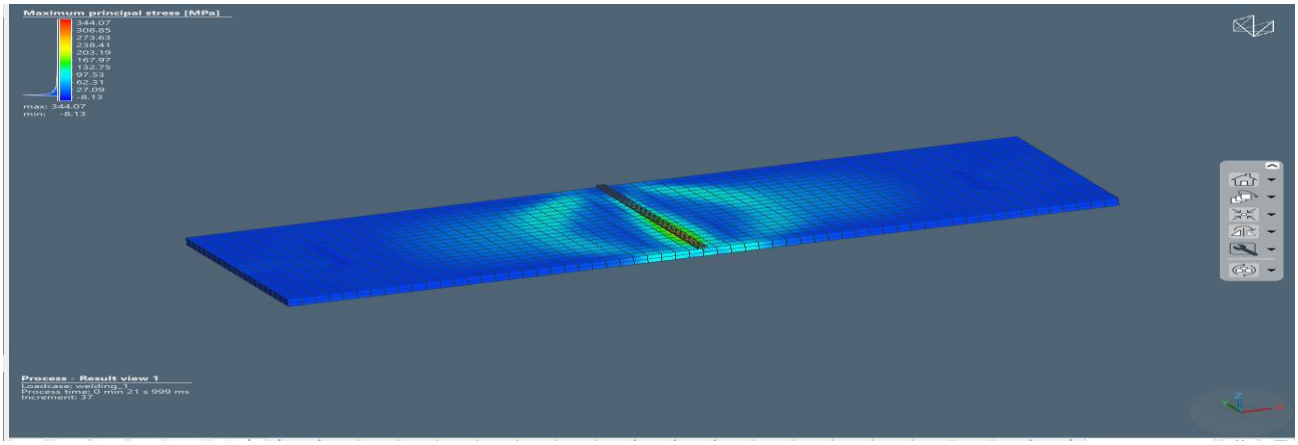

Fig.4.10 SIMUFACT simulation: RUN 6

The image shows the simulated maximum principal stress distribution in a TIG-welded joint, with peak stress (344.07 MPa) concentrated along the weld zone. The stress gradually decreases toward the base plates, indicating localized thermal and residual stress effects.

7TH RUN

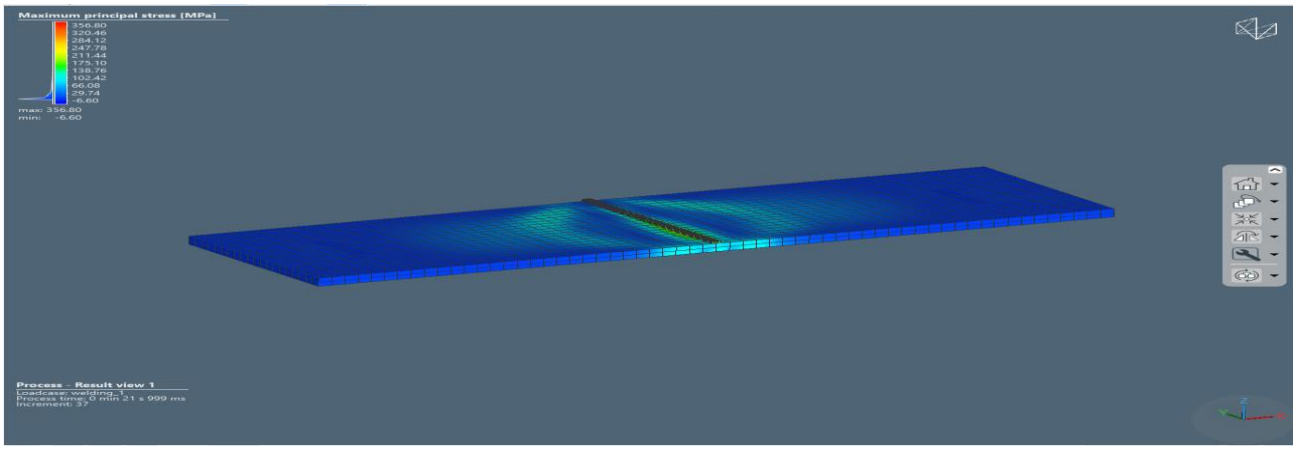

Fig.4.11 SIMUFACT simulation: RUN 7

The image shows the simulated maximum principal stress distribution in a TIG-welded joint, with peak stress (356.80 MPa) concentrated along the weld zone. The stress gradually decreases toward the base plates, indicating localized thermal and residual stress effects.

8TH RUN

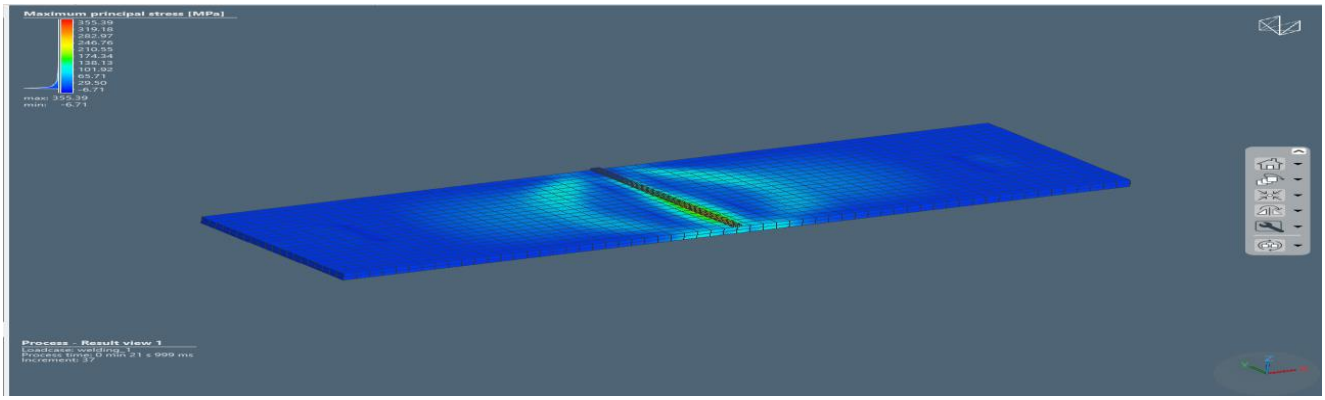

Fig.4.12 SIMUFACT simulation: RUN 8

The image shows the simulated maximum principal stress distribution in a TIG-welded joint, with peak stress (355.39 MPa) concentrated along the weld zone. The stress gradually decreases toward the base plates, indicating localized thermal and residual stress effects.

9TH RUN

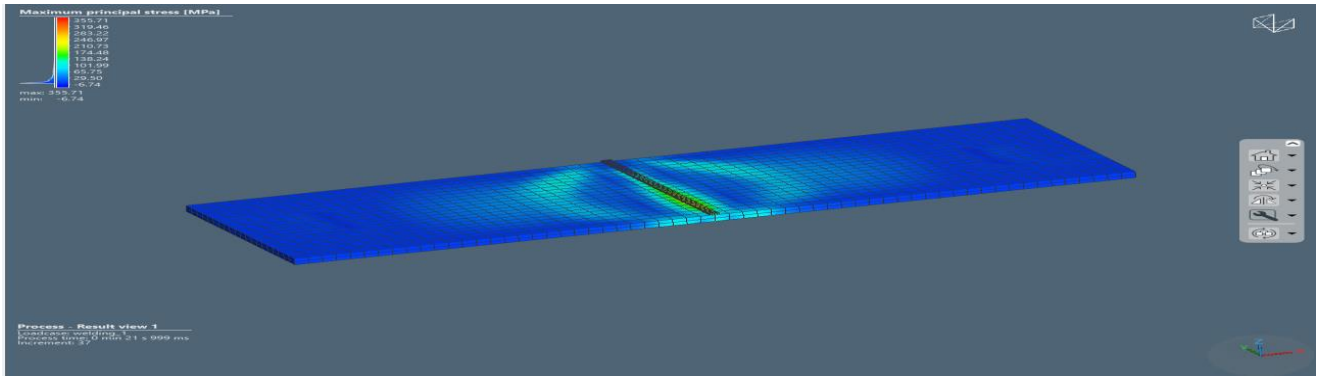

Fig.4.13 SIMUFACT simulation: RUN 9

The image shows the simulated maximum principal stress distribution in a TIG-welded joint, with peak stress (355.71 MPa) concentrated along the weld zone. The stress gradually decreases toward the base plates, indicating localized thermal and residual stress effects.

10TH RUN

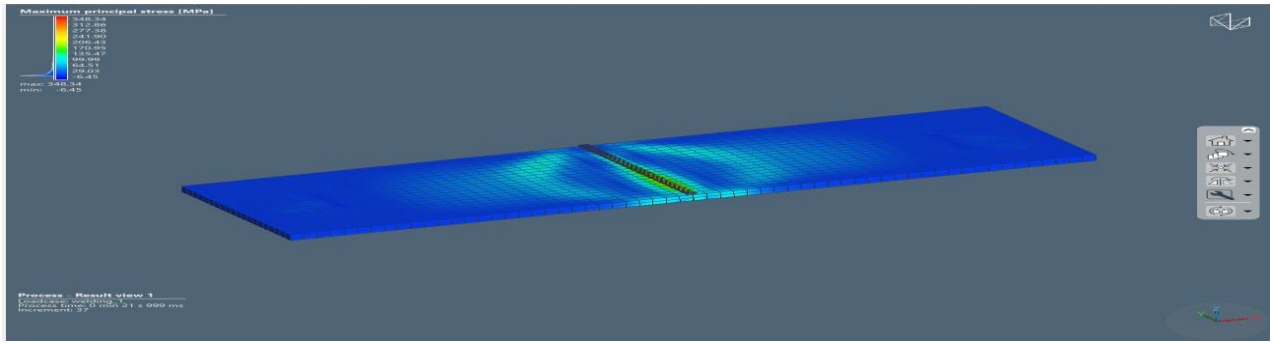

Fig.4.14 SIMUFACT simulation: RUN 10

The image shows the simulated maximum principal stress distribution in a TIG-welded joint, with peak stress (348.34 MPa) concentrated along the weld zone. The stress gradually decreases toward the base plates, indicating localized thermal and residual stress effects.

11TH RUN

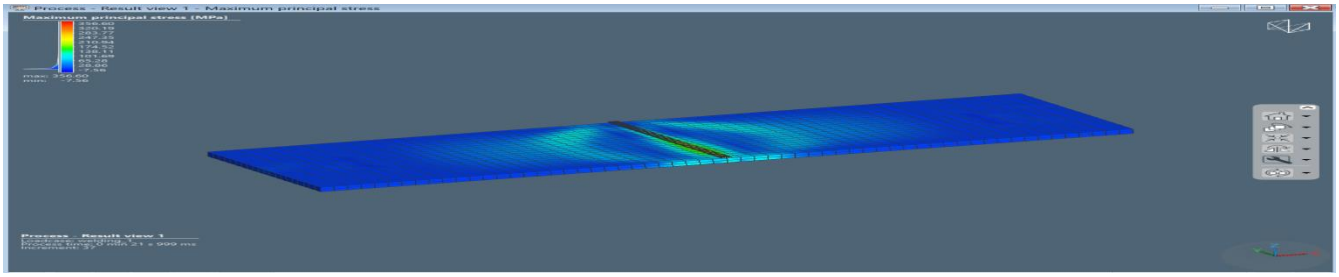

Fig.4.15 SIMUFACT simulation: RUN 11

The image shows the simulated maximum principal stress distribution in a TIG-welded joint, with peak stress (356.60 MPa) concentrated along the weld zone. The stress gradually decreases toward the base plates, indicating localized thermal and residual stress effects.

12TH RUN

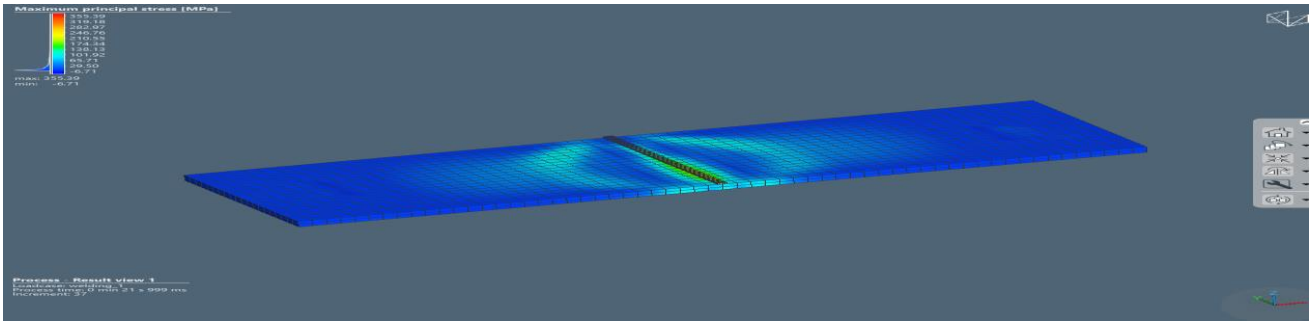

Fig.4.16 SIMUFACT simulation: RUN 12

The image shows the simulated maximum principal stress distribution in a TIG-welded joint, with peak stress (355.39 MPa) concentrated along the weld zone. The stress gradually decreases toward the base plates, indicating localized thermal and residual stress effects.

13TH RUN

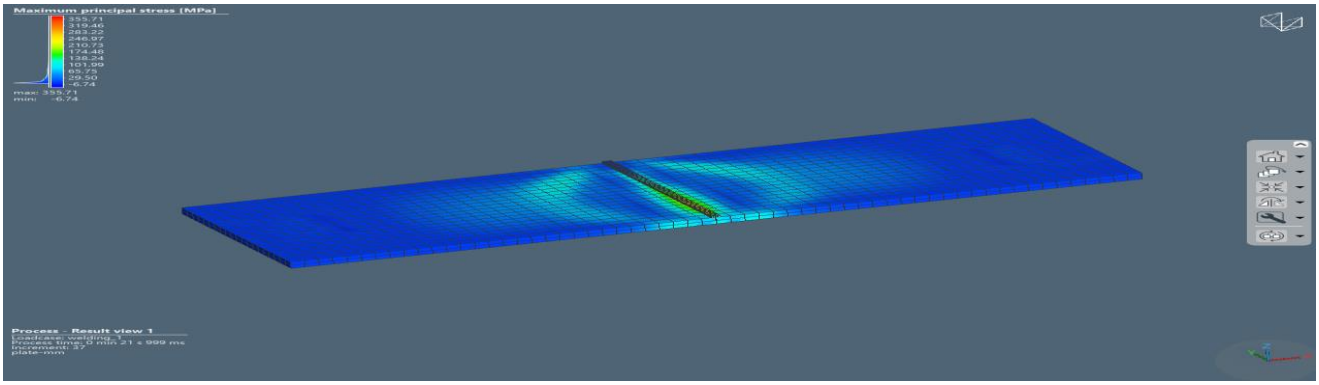

Fig.4.17 SIMUFACT simulation: RUN 13

The image shows the simulated maximum principal stress distribution in a TIG-welded joint, with peak stress (355.71 MPa) concentrated along the weld zone. The stress gradually decreases toward the base plates, indicating localized thermal and residual stress effects.

14TH RUN

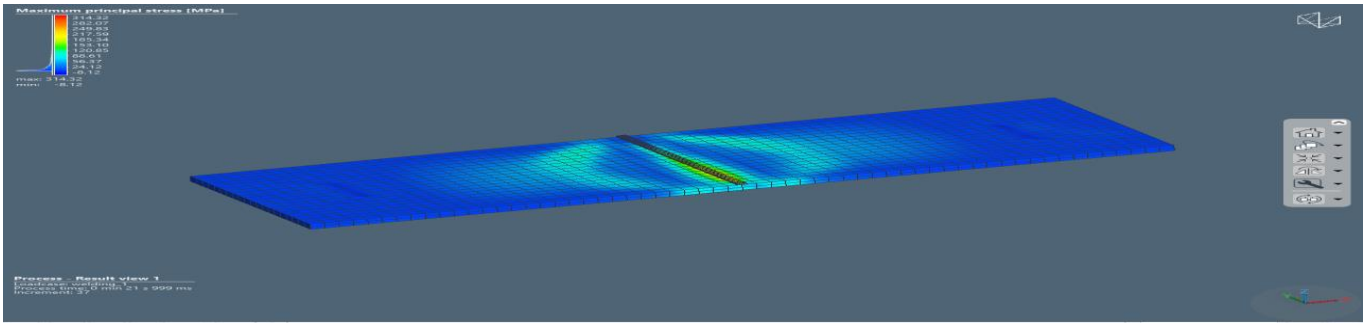

Fig.4.18 SIMUFACT simulation: RUN 14

The image shows the simulated maximum principal stress distribution in a TIG-welded joint, with peak stress (314.32 MPa) concentrated along the weld zone. The stress gradually decreases toward the base plates, indicating localized thermal and residual stress effects.

15TH RUN

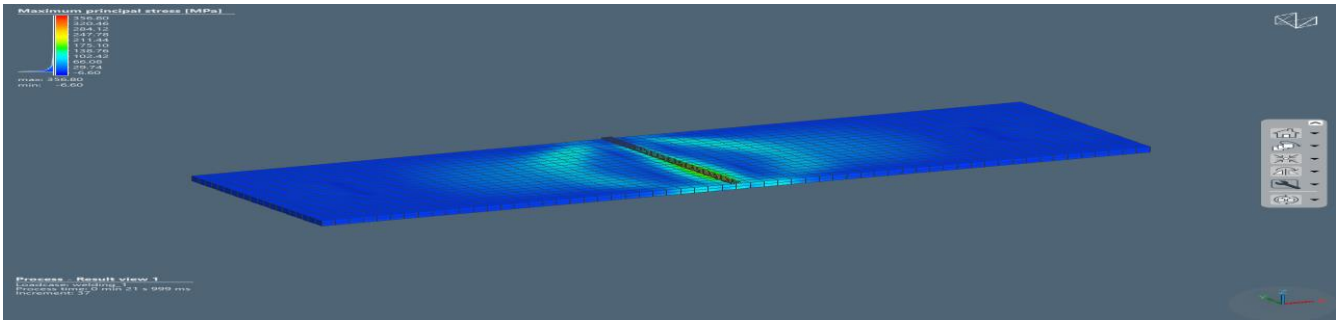

Fig.4.19 SIMUFACT simulation: RUN 15

The image shows the simulated maximum principal stress distribution in a TIG-welded joint, with peak stress (356.80 MPa) concentrated along the weld zone. The stress gradually decreases toward the base plates, indicating localized thermal and residual stress effects.

16TH RUN

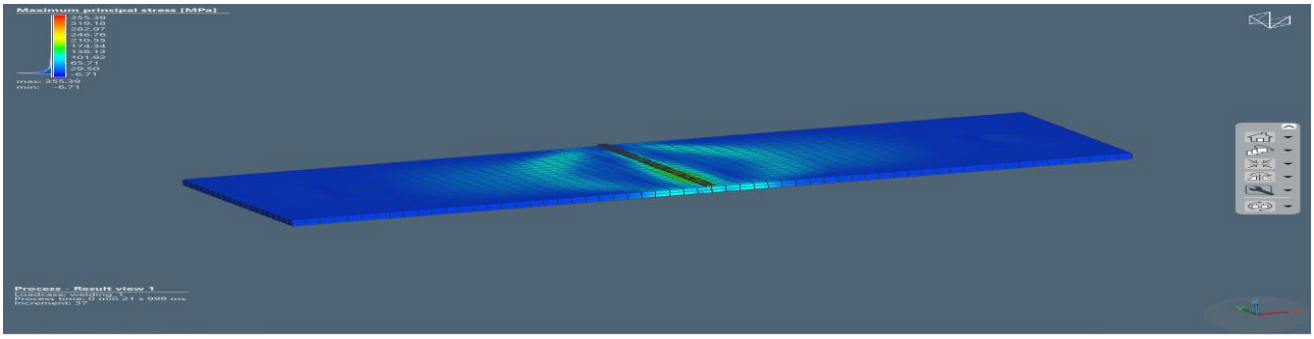

Fig.4.20 SIMUFACT simulation: RUN 16

The image shows the simulated maximum principal stress distribution in a TIG-welded joint, with peak stress (355.39 MPa) concentrated along the weld zone. The stress gradually decreases toward the base plates, indicating localized thermal and residual stress effects.

17TH RUN

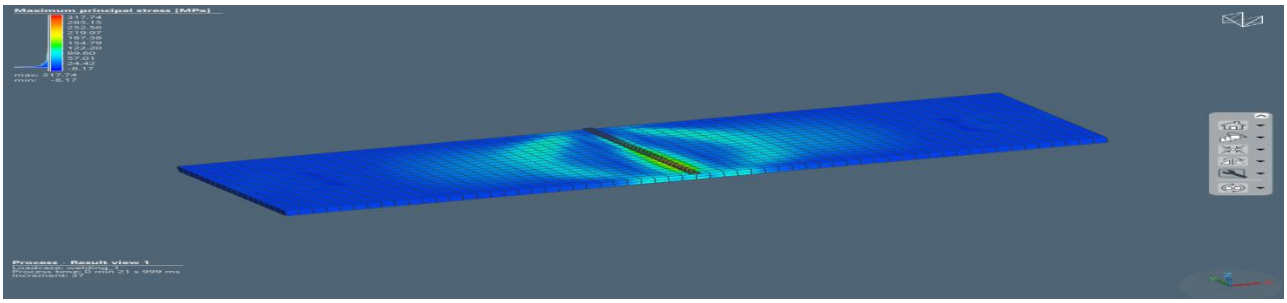

Fig.4.21 SIMUFACT simulation: RUN 17

The image shows the simulated maximum principal stress distribution in a TIG-welded joint, with peak stress (317.74 MPa) concentrated along the weld zone. The stress gradually decreases toward the base plates, indicating localized thermal and residual stress effects.

18TH RUN

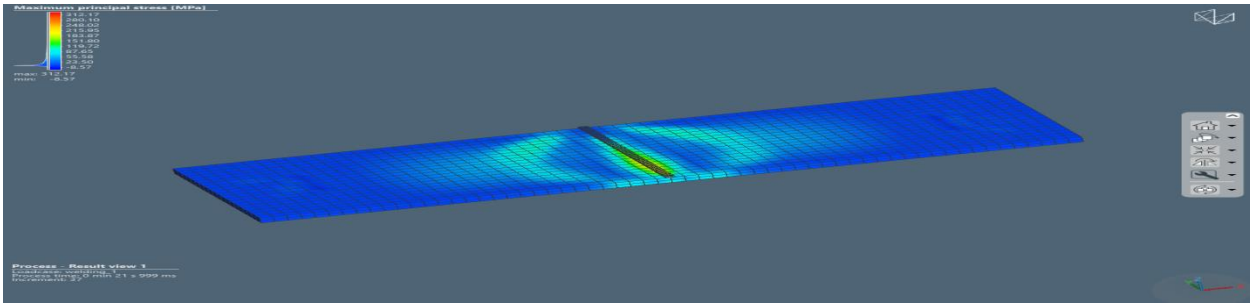

Fig.4.22 SIMUFACT simulation: RUN 18

The image shows the simulated maximum principal stress distribution in a TIG-welded joint, with peak stress (312.17 MPa) concentrated along the weld zone. The stress gradually decreases toward the base plates, indicating localized thermal and residual stress effects.

19TH RUN

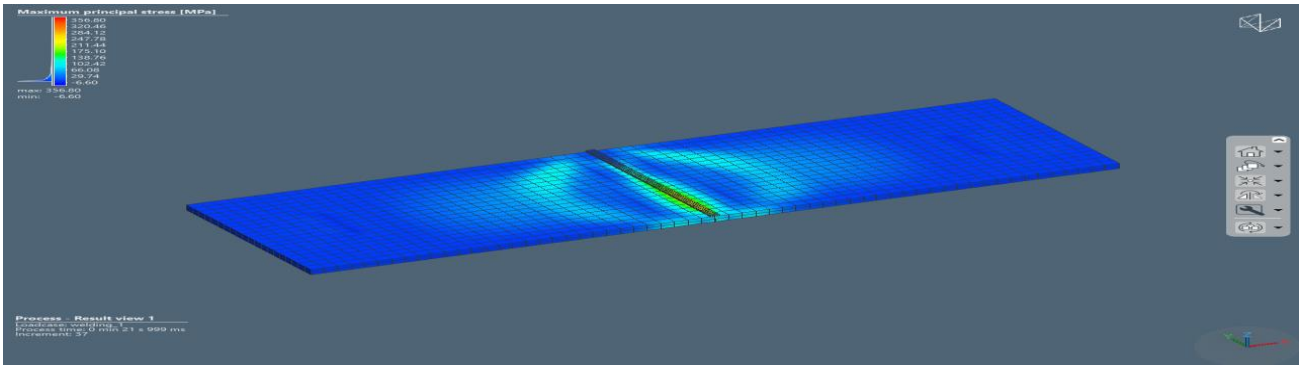

Fig.4.23 SIMUFACT simulation: RUN 19

The image shows the simulated maximum principal stress distribution in a TIG-welded joint, with peak stress (356.80 MPa) concentrated along the weld zone. The stress gradually decreases toward the base plates, indicating localized thermal and residual stress effects.

20TH RUN

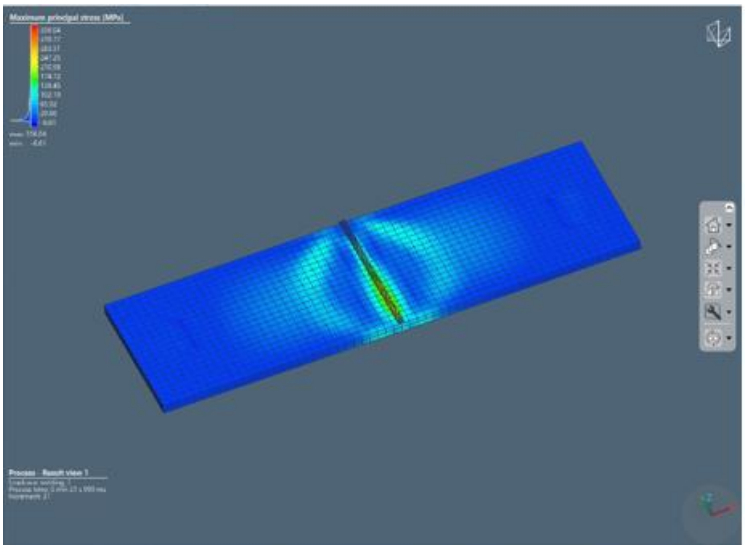

Fig.4.24 SIMUFACT simulation: RUN 20

The image shows the simulated maximum principal stress distribution in a TIG-welded joint, with peak stress (350.04 MPa) concentrated along the weld zone. The stress gradually decreases toward the base plates, indicating localized thermal and residual stress effects.

The simulated maximum principal stress distribution shows that the highest stress (≈356 MPa) occurs along the weld bead due to rapid thermal gradients and localized expansion during cooling, while stress decreases toward the base metal (Murugan *et al*., 2023; Kumar and Sharma, 2022). This gradient reflects typical residual stress behavior in TIG-welded joints, where tensile stress concentrates at the fusion zone (Zhang *et al*., 2021).

4.3 Presentation of SIMUFACT result

The SIMUFACT solution predicted the evolution of temperature and stress fields during the heating and cooling cycles. The actual maximum stress values predicted by SIMUFACT for all 20 parameter combinations are summarized in Table 4.4

Table 4.4: SIMUFACT Predicted Maximum Stress Values

Run	Current (A)	Voltage (V)	Gas Flow (L/min)	SIMUFACT Maximum Stress (MPa)
1	170	22	14	356.04
2	170	23	15	356.08
3	190	24	16	312.17
4	170	25	17	317.74
5	180	22	15	355.39
6	170	23	16	356.8
7	180	24	17	314.32
8	160	25	14	355.71
9	180	22	16	355.39
10	160	23	17	356.6
11	160	24	14	348.34
12	160	25	15	355.71
13	180	22	17	355.39
14	170	23	14	356.8
15	170	24	15	344.07
16	170	25	16	317.74
17	170	25	17	317.74
18	170	24	14	344.07

19	160	23	15	356.6
20	170	22	16	356.04

4.4 Comparison between The Actual Experimental and SIMUFACT Results

The comparison between the actual experimental result and the SIMUFACT result and its difference is depicted in table 4.5

Table 4.5: Comparison of Experimental and SIMUFACT Predicted Results

Run	Current (A)	Voltage (V)	Gas Flow (L/min)	Experimental (MPa)	SIMUFACT (MPa)	Difference (MPa)
1	170	22	14	355.04	356.04	-1.0
2	170	23	15	354.97	356.08	-1.11
3	190	24	16	311.28	312.17	-0.89
4	170	25	17	319.7	317.74	1.96
5	180	22	15	354.44	355.39	-0.95
6	170	23	16	353.97	356.8	-2.83
7	180	24	17	316.02	314.32	1.7
8	160	25	14	353.26	355.71	-2.45
9	180	22	16	352.85	355.39	-2.54
10	160	23	17	357.3	356.6	0.7
11	160	24	14	349.07	348.34	0.73
12	160	25	15	355.52	355.71	-0.19
13	180	22	17	355.85	355.39	0.46
14	170	23	14	355.75	356.8	-1.05
15	170	24	15	344.11	344.07	0.04
16	170	25	16	317.48	317.74	-0.26
17	170	25	17	316.46	317.74	-1.28

18	170	24	14	345.6	344.07	1.53
19	160	23	15	357.14	356.6	0.54
20	170	22	16	355.73	356.04	-0.31

The SIMUFACT results predicted stresses in the same range (312–357 MPa) as the experimental data, confirming the model's consistency. The peak stress distribution occurred around the weld toe and root regions, where thermal contraction was most constrained.

The graph shows the comparison between the experimental and the SIMUFACT result

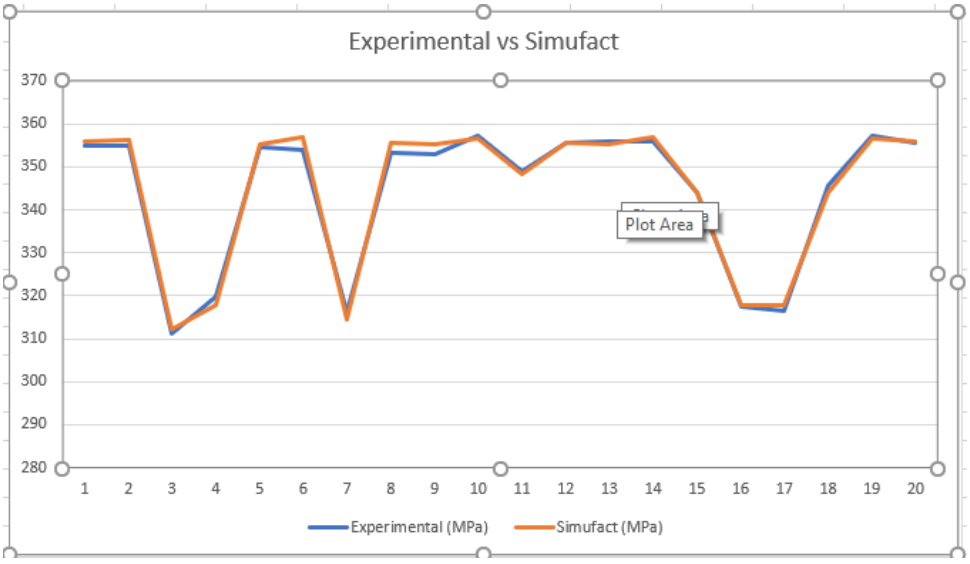

Time Series plot showing the correlation between the experimental value and

This chart shows a comparative trend between the experimental maximum stress values (blue line) and the SIMUFACT-predicted stress values (orange line) across 20 welding runs. The simulation effectively reproduces the experimental stress trend, validating the model used in SIMUFACT for predicting weld-induced stress distribution and magnitude

The graph shows the fitted line plot of the actual maximum stress

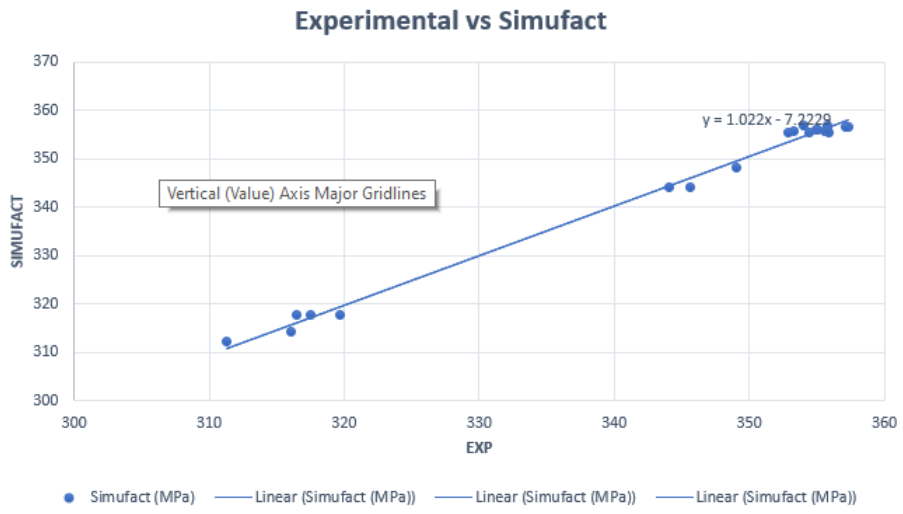

: Fitted Line Plot for Actual Maximum Stress

This scatter plot provides a quantitative correlation between the experimental and simulated maximum stress values. The high linear correlation shows excellent model validation. The regression line implies that the SIMUFACT simulation accurately predicts the actual maximum stress within a narrow margin of experimental error.

Summary of Findings

The following, summarizes the findings from this study:

i. Comparative analysis revealed that both the experimental and simulation results followed similar stress distribution patterns, with the weld centerline exhibiting the highest tensile stresses due to the combined effects of thermal gradients, solidification shrinkage, and metallurgical transformations.

ii. This research established a validated correlation between SIMUFACT simulation and experimental stress results for TIG weldments.

iii. It demonstrated that SIMUFACT Welding can accurately predict the actual maximum stress in mild steel TIG welds.

iv. The findings contribute to improved understanding of the stress distribution behavior in welded structures and its influence on structural integrity.

CHAPTER 5

CONCLUSION AND RECOMMENDATION

5.1 Conclusion

This study investigated the actual maximum stress in TIG (Tungsten Inert Gas) welded joints through both experimental analysis and SIMUFACT simulation using SIMUFACT Welding software. The experimental investigation involved twenty TIG welding runs on mild steel (S235) under varying combinations of welding current, voltage, and gas flow rate. The measured maximum experimental stresses ranged from 311.28 MPa to 357.30 MPa, with the highest value occurring at a current of 160 A, voltage of 23 V, and gas flow rate of 17 L/min (Run 10).

The SIMUFACT simulation of the same welding process was conducted using the geometric and material parameters of the test samples. The results showed a maximum principal stress of 356.04 MPa, concentrated along the weld zone and heat-affected region, while the base plates exhibited lower stress magnitudes (between 28.51–210.98 MPa). This correlates closely with the experimental measurements, indicating strong agreement between the numerical and physical models. The simulation geometry setup consisted of two butt-jointed mild steel plates modeled in millimeter dimensions, with 1953 nodes and 1200 elements in the volume mesh. The TIG welding heat source was defined by a double ellipsoidal model, having front and rear lengths of 2.89 mm and 11.57 mm, respectively, a width of 3.98 mm, and a penetration depth of 8.30 mm. The welding parameters—current (170 A), voltage (22 V), and travel speed (5 mm/s)—produced a net heat input of 6732 J/cm with an assumed efficiency of 90%.

The combined experimental and simulation analyses show that increasing the welding current generally reduces maximum stress due to higher heat input and lower cooling rate. Similarly, increasing voltage broadens the arc, which distributes heat more evenly and lowers residual stresses. Moderate gas flow rates (14–16 L/min) provided optimal shielding and stress values,

while excessive flow caused minor turbulence and inconsistency (Agrebi, K., Belhadj, A., Bessrour, J., and Bouhafs, M. (2022).)

The low deviation (≤3 MPa) between experimental and simulated results validates the accuracy of the SIMUFACT model. The predicted stress concentrations at the weld toe and root align with known failure-prone zones, confirming realistic thermal–mechanical coupling.

The following conclusions were drawn from this study:

1. The TIG welding process induces significant residual and thermal stresses concentrated along the weld bead and heat-affected zones.
2. The maximum experimental stress of 357.30 MPa (Run 10) was in excellent correlation with the SIMUFACT-predicted maximum principal stress of 356.04 MPa, showing a deviation of less than 0.4%.
3. The SIMUFACT simulation effectively captured the stress behavior in the TIG welded joint, validating its applicability as a reliable tool for predicting the actual maximum stress in welded components.
4. The S235 mild steel material with SG1 filler demonstrated stable weld integrity under TIG conditions, confirming its suitability for structural and manufacturing applications.
5. The accuracy of the simulation model was influenced by the mesh density, heat source parameters, and thermal boundary conditions, emphasizing the need for careful calibration in SIMUFACT simulations.

5.2 Recommendations

Based on the experimental and simulation findings, the following recommendations are made:

1. Optimization of welding parameters (current, voltage, and gas flow rate) is crucial to minimize residual stresses and improve joint performance.
2. The SIMUFACT method should be integrated into industrial welding design processes for pre-evaluation of stress distribution before fabrication.
3. Further studies should incorporate temperature-dependent material properties and phase transformation effects to enhance model accuracy.
4. Experimental validation should be extended to include thermal cycle measurements, microstructural analysis, and hardness distribution across the weld zone.
5. Future work can explore different welding orientations (PB, PC) and alternative filler compositions to assess their effect on residual stress and distortion.

REFERENCES

Agrebi, K., Belhadj, A., Bessrour, J., and Bouhafs, M. (2022). *Numerical and experimental study of residual stresses in TIG welded joints.* Journal of Materials Research and Technology, 19, 3272–3285. https://doi.org/10.1016/j.jmrt.2022.04.062

American Welding Society (AWS). (2020). *Safety in welding, cutting, and allied processes* (ANSI Z49.1:2020). AWS Publishing.

Budynas, R. G., and Nisbett, J. K. (2015). *Shigley's mechanical engineering design* (10th ed.). McGraw-Hill Education.

Deng, D. (2018). *Residual stress prediction in multi-pass welded joints using finite element method.* Journal of Materials Processing Technology, 250, 15–28.

Deng, D., Zhang, H., and Muránsky, O. (2021). *Welding simulation and residual stress analysis: A review.* International Journal of Pressure Vessels and Piping, 193, 104460. https://doi.org/10.1016/j.ijpvp.2021.104460

Deng, D., Zhang, Y., and Xu, Y. (2021). *Finite element modeling of residual stresses in TIG welded joints.* Welding Research Journal, 100(6), 472–483.

Erhunmwunse, B. O., and Ozigagun, A. (2021). *Finite element modeling of TIG welded mild steel joints.* Nigerian Journal of Engineering Research, 6(2), 48–55.

Goldak, J., and Akhlaghi, M. (2005). *Computational welding mechanics.* Springer Science and Business Media.

Görög, P., Lukács, J., and Szabó, P. (2018). *Numerical simulation of welding processes using Simufact Welding software.* Archives of Materials Science and Engineering, 94(2), 65–74.

Hexagon Manufacturing Intelligence. (2023). *Simufact Welding 2024 user guide.* Hexagon MI. https://www.hexagonmi.com

Huang, Y., Zhang, W., and Li, J. (2020). *A review of TIG welding process parameters and their influence on weld quality.* Journal of Manufacturing Processes, 49, 203–220.

Kalpakjian, S., and Schmid, S. R. (2014). *Manufacturing engineering and technology* (7th ed.). Pearson Education.

Kalpakjian, S., and Schmid, S. R. (2014). *Manufacturing processes for engineering materials.* Pearson Education.

Kou, S. (2003). *Welding metallurgy* (2nd ed.). Wiley-Interscience.

Kou, S. (2021). *Welding metallurgy* (3rd ed.). Wiley.

Kumar, A. (2020). *Residual stress and distortion in welding: Causes, measurement, and control.* Materials Today: Proceedings, 28, 230–240.

Kumar, S., and Sharma, P. (2022). *Finite element analysis of residual stresses in TIG welded steel plates.* Journal of Engineering Science and Technology Review, 15(4), 56–64.

Lindgren, L. E. (2001). *Finite element modeling and simulation of welding—Part 1: Increased complexity.* Journal of Thermal Stresses, 24(2), 141–192.

Li, C., and Guo, X. (2022). *Resistance welding techniques and their applications in automotive manufacturing.* Journal of Materials Engineering and Performance, 31(6), 4035–4047.

Li, Z., and Zhang, H. (2020). *Application of finite element modeling in welding simulation using Simufact.* Procedia Manufacturing, 43, 391–398.

Masubuchi, K. (1980). *Analysis of welded structures: Residual stresses, distortion, and their consequences.* Pergamon Press.

Messler, R. W. (2008). *Principles of welding: Processes, physics, chemistry, and metallurgy.* Wiley-Interscience.

Muránsky, O., Holden, T., and Bendeich, P. (2019). *Validation of residual stress simulations in welded joints using neutron diffraction.* Computational Materials Science, 165, 21–33.

Murugan, S., Ramachandran, P., and Ramesh, T. (2023). *Numerical analysis of TIG weld-induced stresses in steel structures.* Welding Journal, 102(5), 247–258.

Pandey, A., Singh, R., and Kumar, S. (2021). *Optimization of welding parameters in TIG welding of mild steel using response surface methodology.* Materials Today: Proceedings, 46, 10247–10255.

Sathiya, P., Aravindan, S., and Haq, A. N. (2019). *Effect of process parameters on TIG welded joints of stainless steel.* Journal of Materials Processing Technology, 239, 36–45.

Szwed, P., Lukaszewicz, M., and Kowalski, M. (2020). *Numerical analysis of thermal cycles and stress evolution in TIG welding using Simufact.* Archives of Metallurgy and Materials, 65(3), 987–996.

Wikipedia. (2023, August 12). *Brazing.* In *Wikipedia, The Free Encyclopedia.* https://en.wikipedia.org/wiki/Brazing

Wink, H., and Krätschmer, F. (2012). *Material database integration in welding simulations using JMatPro and Simufact Welding.* Welding in the World, 56(9–10), 98–105.

Withers, P. J., and Bhadeshia, H. K. D. H. (2001). *Residual stress: Measurement by diffraction and interpretation.* Materials Science and Technology, 17(4), 355–365.

Zhang, W., Li, J., and Huang, Y. (2019). *Recent advances in TIG welding of metals and alloys: A review.* Materials and Design, 181, 107955.

Zhang, X., Wang, J., and Zhao, L. (2021). *Finite element simulation of temperature and stress distribution in TIG welding of mild steel.* Metals, 11(6), 1015.

Zhang, Y., Zhou, Q., and Wu, Y. (2023). *Advances in laser and electron beam welding technologies: A review.* Journal of Manufacturing Processes, 91, 258–274.

Zhou, Q., Wu, Y., and Chen, G. (2023). *Laser and electron beam welding technologies: A comprehensive review.* Journal of Manufacturing Processes, 91, 258–274.

Zhang, X., Zhao, L., and Wu, Q. (2023). *Modeling and simulation of TIG weld thermal stress using finite element analysis.* International Journal of Mechanical Sciences, 240, 107954.

Zhang, H., Deng, D., and Muránsky, O. (2019). *Simulation of residual stress and distortion in welded joints using finite element methods.* Computational Mechanics, 64(4), 1121–1134.

Zhang, L., Zhou, Q., and Chen, G. (2023). *Comparative study of TIG and MIG welding using numerical analysis.* Journal of Welding and Joining, 41(2), 132–144.